Dissertation zur Erlangung des Doktorgrades der Fakultät für Chemie und Pharmazie der Ludwig-Maximilians-Universität München

---

Novel Treatment Strategies and Mechanisms of Actin Binding Compounds in Cancer Therapy

---

Christina Moser

aus

Krasnojarsk, Russland

2017

ERKLÄRUNG

Diese Dissertation wurde im Sinne von § 7 der Promotionsordnung vom 28. November 2011 von Frau Prof. Dr. Angelika M. Vollmar von der Fakultät für Chemie und Pharmazie betreut.

EIDESSTATTLICHE VERSICHERUNG

Diese Dissertation wurde eigenständig und ohne unerlaubte Hilfe erarbeitet.

München, den 08.05.2017

.....
Christina Moser

Dissertation eingereicht am:	24.03.2017
1. Gutachterin:	Prof. Dr. Angelika M. Vollmar
2. Gutachter:	Prof. Dr. Stefan Zahler
Mündliche Prüfung am:	25.04.2017

CONTENTS

1 INTRODUCTION

1.1 Cancer and current treatment options

Cancer is the second leading cause of death of humans worldwide and the incidence of suffering from cancer has increased by approximately two million cases from 2008 to 2012.[1] Despite the development of detecting cancer early, the improved pharmacological and surgery treatment as well as healthier life styles, fighting cancer is still one of the greatest burdens in modern medicine. Not only risk factors such as tobacco, obesity and chronic infections, but also epidemiological influences and the genetic background have an impact on cancer incidence and are challenges for cancer treatment.[1] Radiation and pharmacological medication are, after surgery, the state of the art treatment of tumors.[2] Among others, the treatment strategies of breast cancer have made progress over the last years. Prominent chemotherapeutic strategies in breast cancer treatment are hormone targeted therapy, for example with the estrogen receptor modulator tamoxifen.[3] Also antibodies against growth factor receptors, like trastuzumab are in clinical use.[4] Furthermore, research focuses more on prophylactic vaccination of infection dependent tumor development, as it is the case for hepatitis B and human papilloma viruses.[5] Nevertheless, classic chemotherapy, such as the anthracycline-antibiotic, doxorubicin and taxanes like paclitaxel are still in use and are an important part in clinical treatment.[6] The malignant transformation of a mammalian cell could be induced by cancerogenous factors, such as chemicals, radiation and viruses. Cancer is a multifactorial disease and more than one genetic alteration of a human cell is necessary to develop malignancy.[7] Thus, the commonly used pharmacological high dose monotherapy, wherein the tumor survival capacity is targeted unspecifically, seems to be outdated and novel therapeutic options are needed. For instance, doxorubicin was proven to be more effective in combination therapy with the DNA alkylating agent ifosfamide in comparison to single treatment.[8] Hence, combination treatments of two or more chemotherapeutics are promising approaches for advanced cancer therapy, since they reduce the probability

of resistance mechanisms in cancer. In addition, many pharmacological therapies induce strong side effects, e. g., nausea, hair loss, or even neurotoxicity and cardiotoxicity, which impair quality of life and affect life expectancy.[9] Besides doxorubicin, cytoskeletal affecting drugs such as microtubule targeting paclitaxel are often used in pharmacological treatment of cancer, but are still accompanied by strong side effects, like peripheral neuropathy.[10]

A further hallmark of many types of cancer is the metastatic dissemination of cells. Herein, cells of the primary tumor undergo transformation and obtain a motile and invasive phenotype.[11] One example for a chemotherapeutic drug, which targets the metastatic dissemination of cancer cells, is the Src tyrosine kinase family inhibitor saracatinib. It successfully inhibits the extravasation of metastatic tumor cells resulting in inhibition of breast cancer brain-metastasis in the clinic.[12] Despite promising investigations for the inhibition of metastasis in cancers, such as the integrin inhibitor cilengitide, new options and approaches for cancer therapy are urgently needed.[13,14]

1.2 Actin cytoskeleton as potential target

1.2.1 Actin structure and physiological function

One promising target for new therapeutic approaches in cancer treatment is the cytoskeleton of tumor cells. The cytoskeleton consists of three different structural components, which interact with each other and build a dynamically regulated three dimensional network. The cytoskeleton network is characterized by associating and dissociating monomer units, which polymerize or depolymerize to filament structures.[15] In comparison to the intermediary filaments (10 nm) and microtubules (25 nm), the actin filaments are the smallest components of the cytoskeleton, with a diameter of 7 nm. Actin is a 42 kDa globular expressed protein with three different isoforms. Fifty percent of all proteins contained in the muscles is α-actin, whereas β- and γ-actin occur in non-muscle tissue and function as mechanical stabilizer for cell shape, cell migration, and intracellular transport processes.[16] The actin structures build a contractile ring during cytokinesis of mammalian cells and are therefore crucial for cell division and proliferation. During cell migration actin participates in the formation of cellular protrusions and is

responsible for cellular contractility.[17] Besides the cytoplasmic form, actin is also present in the nucleus of mammalian cells and plays an important role in modulatory processes, like the regulation of transcription by interacting with RNA-polymerases,[18,19] and nuclear translocation of the transcription co-activator MRTF-A,[20] as well as chromatin remodeling.[21] There are also some hints that nuclear actin might participate in the DNA damage repair machinery.[22,23]

The polymerization of actin filaments is a very dynamic process. A minimum of four G-actin subunits assemble spontaneously or through actin binding proteins to the nucleation complex, which further builds actin filaments (F-actin) by adding of ATP bound G-actin subunits.[24] The polymerization is faster at the barbed end, whereas depolymerization proceeds predominantly at the pointed end.[25] More complex structures of actin are formed by additional actin regulating proteins.[25,26] For example, gelsolin or cofilin/actin depolymerizing factor bind to F-actin, followed by severing and actuating the actin depolymerization. Furthermore, capping proteins block the barbed end and inhibit the elongation of F-actin. Branched actin filaments are important at the leading edge of motile and migrating cells. In addition, the actin polymerizing complex Arp2/3 is an important regulator of actin dynamics and facilitates the assembly of new filaments in an angle of 70° to existing filaments (Figure 1.1).[15,25] Since decades it is known that natural compounds like phalloidin or cytochalasin D have an impact on actin dynamics.[27]

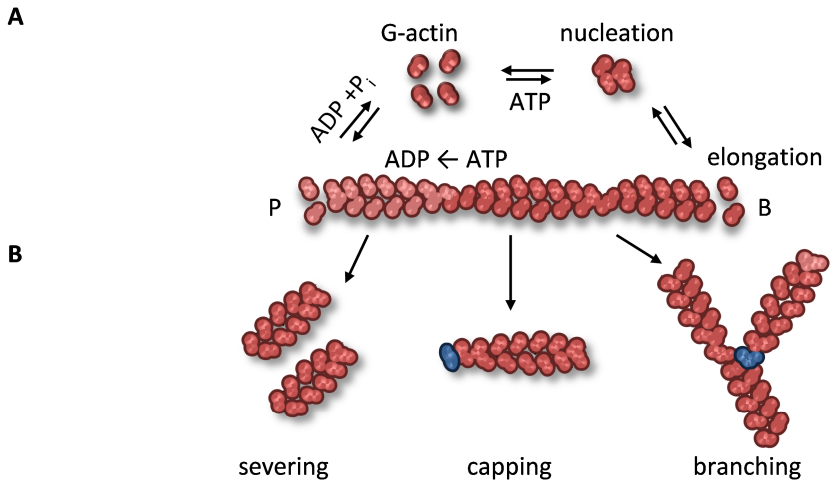

Figure 1.1: The actin structure and its dynamics. A: Four G-actin monomers assemble with ATP to the nucleation complex, which starts the actin polymerization. The elongation of F-actin is faster at the barbed end (B) in comparison to the pointed end (P). ATP is hydrolyzed to ADP followed by depolymerization predominantly at the pointed end. The exchange of ADP to ATP of G-actin restarts actin polymerization. **B:** Actin binding proteins regulate the severing, capping and branching of F-actin.

1.2.2 The actin binding compounds chondramide B and miuraenamide A

Compounds from different natural sources such as plants, marine organisms, and microorganisms have been applied for centuries in the treatment of cancer and infectious diseases.[28] The natural compounds and their derivatives represent the major part of anti-cancer drugs used in clinics and a high number of natural compound-derived substances currently undergo clinical trials.[29] One important source of potent substances are myxobacteria.[30] For instance, the epothilone from *Sorangium cellulosum* is in clinical use for breast cancer treatment and underlines the potency of natural compounds derived from myxobacteria, targeting the cytoskeleton.[31] Two further examples of myxobacteria-derived natural compounds are chondramide and miuraenamide.

Chondramides are cyclodepsipeptides (Figure 1.2 A), which are produced by the myxobacteria strain *Chondromyces crocatus.* First studies with chondramide indicated cytostatic effects on carcinoma cell lines by affecting the actin cytoskeleton dynamics.[32] We recently demonstrated the very specific *in vitro* effects on breast cancer cell lines in comparison to non-cancer cells.[33] Further studies on the metastatic inhibitory capacity of chondramide achieved promising results in animal experiments.[34]

Miuraenamides are structurally related to the similarly functioning chondramides. Miuraenamide A (Figure 1.2 B) was isolated in the marine environment in Japan from the halophilic myxobacteria strain *Paraliomyxa miuraensis*. In line with chondramide it has a cyclodepsipeptide structure with a halogen atom. Biological examinations showed an antibiotic activity and inhibitory effects on NADH oxidase in higher doses.[35] Additionally, miuraenamide is able to stabilize the actin cytoskeleton, similar to chondramide, and leads to a disruption of the actin cytoskeleton in different cell lines.[36] The cytotoxic activity of miuraenamide on mammalian cells was briefly examined and achieved promising results *in vitro*.[37] Both compounds are actin stabilizing agents, which lead to a hyperpolymerization of actin followed by an actin agglomeration in the cytoplasm of mammalian cells.[32,36]

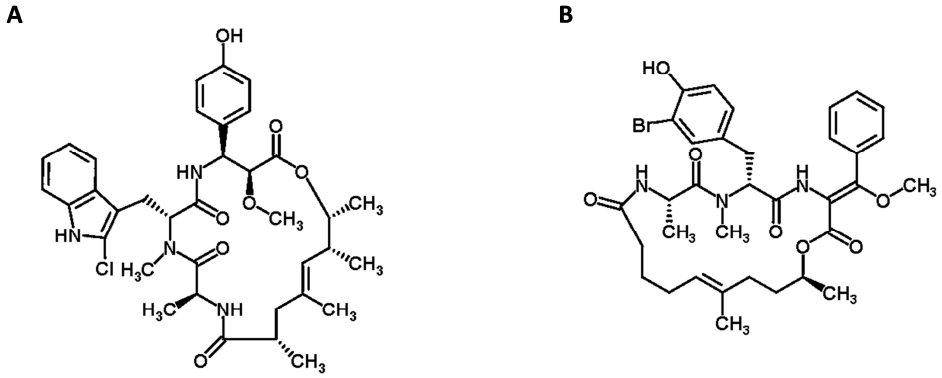

Figure 1.2: The chemical structure of two actin binding compounds. A: Chondramide B[38] and **B:** Miuraenamide A[35].

1.3 DNA damage response (DDR)

Mammalian cells could encounter DNA damages through different stimuli and have to react with repair mechanisms. The cells which fail to repair their DNA damages, initiate apoptosis in the final instance. As an example, the DNA damage occurs during the replication, where the DNA double strands have to be unwound, broken, and rejoined by the topoisomerase II for sufficient DNA replication.[39] Disruption of this replication process ends up in DNA double strand breaks (DSB).[40] Exogenous factors like the exposure to radiation or chemicals induce mutagenic alteration of the DNA. Thus, mammalian cells have a tightly regulated repair machinery to initiate the response mechanisms and to avoid extensive damages of the DNA. The initial step of DNA damage response (DDR) is the recognition of DNA lesions by activated repair proteins, which attach on the damage

site of the DNA strand. For instance, important DNA repair downstream kinases are the ataxia telangiectasia mutated (ATM) or ATR (ATM- and Rad3-related) proteins in homologous recombination and the Ku/DNA-dependent protein kinase (DNA-PK) catalytic subunit complex in non-homologous end-joining.[41] Furthermore, the activation of DNA-PK by autophosphorylation not only results in repair complex formation, but also in the activation of telomere regulation[42] and changes of the Golgi structure.[43] Those repair enzymes could phosphorylate the histone 2A.x (γH2A.x) amongst others, which is a predictor for DSB and the recruiter of the repair machinery.[44] The tightly regulated DDR was discussed to be influenced by alterations of the actin dynamics.[23]

1.3.1 DDR via the Golgi complex

The Golgi complex primarily coordinates the sorting and secretion of proteins and is associated to the actin cytoskeleton. In 2009, the group of Field published the alteration of Golgi constellation around the nucleus, influenced by a DNA damage signaling cascade depending on actin network as a transmission system.[43,45] The Golgi membrane is anchored to the actin cytoskeleton via a complex of transmitting proteins. Following the induction of DNA damage by radiation or chemicals, the repair kinase DNA-PK is activated. Further on, the DNA-PK phosphorylates the Golgi phosphoprotein 3 (GOLPH3) at Thr143/Thr148 residues, which is linked to the Golgi membrane via the phosphatidylinositol-4-phosphate (PI4P).[45] Under physiological conditions, the phosphorylation drives the binding of GOLPH3 to the unconventional myosin 18A (Myo18A) and increases the Golgi area via a tensile force of the associated actin cytoskeleton (Figure 1.3). The Golgi dispersal was described to be independent of apoptosis, but the efficient signaling cascade of the Golgi complex is essential to the survival after DNA damage induction.[43] Thus, the inhibition of Golgi dependent DDR represents a novel promising approach for the combined treatment of DNA damaging and actin binding compounds.

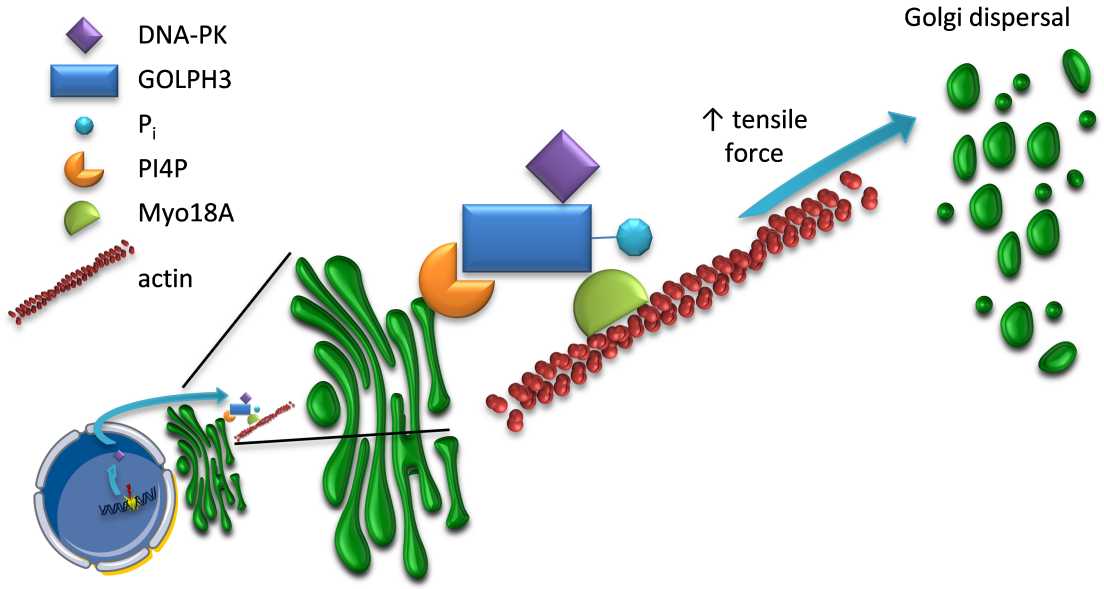

Figure 1.3: The Golgi dispersal signaling cascade after DNA damage induction. The DNA dependent protein kinase (DNA-PK) is activated due to DNA damage and phosphorylates the Golgi phosphoprotein 3 (GOLPH3), which is linked via phosphatidylinositol-4-phosphate (PI4P) to the Golgi membrane (in green). The phosphorylation (P_i) of GOLPH3 induces enhanced binding of the unconventional myosin 18A (Myo18A), which is further linked to the actin cytoskeleton. The signaling cascade, which is activated by DNA damage, induces a tensile force to the Golgi complex and leads to the Golgi dispersal.[46]

1.3.2 The DNA damaging agent doxorubicin

Doxorubicin (Doxo), or adriamycin, is a widely applied chemotherapeutic agent in neoplastic diseases. For instance, it has been clinically used for decades for treatment of various cancer types, including lymphomas, carcinomas, breast and ovarian cancers.[9] It was first isolated from *Streptomyces peucetius*[47] and along with its precursor daunorubicin, Doxo is related to the anthracycline class of antitumor antibiotics. The chemical structure is depicted in Figure 1.4, which shows the characteristic tetracycline part with substituted glycosyl residue. Doxo induces DNA damages by intercalating into the DNA double strand. It inhibits the DNA topoisomerase II by building a complex with the DNA and topoisomerase II, which leads to persistent DNA damage. Under physiological conditions, the topoisomerase II induces DNA double strand breaks to support sufficient DNA replication, transcription, and recombination. Highly proliferating cells, such as tumor cells, express elevated amounts of the enzyme.[48] Another mode of action of Doxo is the formation of reactive oxygen species (ROS), which are mainly produced in the mitochondria. However, the exact mechanism by which Doxo induces

ROS is still under debate. It is supposed that Doxo is converted by the NADPH dehydrogenase of the mitochondrial electron transport chain, to a semiquinone radical. Those effects on mitochondria were discussed to cause the cardiotoxicity. Therefore, the limiting factor of Doxo treatment in clinics is the long-term cardiotoxic effect in patients.[49] However, Doxo is still one of the main chemotherapeutic drugs used in the clinic. This reinforces the need to find novel combination partners for Doxo in order to lower side effects in patients.

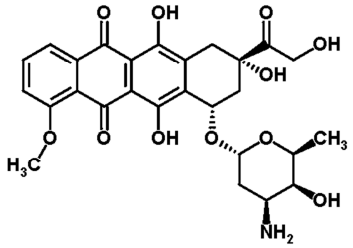

Figure 1.4: Chemical structure of doxorubicin.[47]

1.4 Cell migration

Besides the regulation of DDR mechanisms, actin also participates in the migration of mammalian cells. The migration of cells is crucial for physiological processes such as embryogenesis, immune response, and the building of blood vessels.[50] However, migration also participates in the development of pathophysiological processes, above all tumorigenesis and the formation of metastasis.[11] The cell locomotion consists of different steps, and two dimensional (2D) migration differs from the migration in a three dimensional (3D) environment.[51] During the movement over a 2D substrate, the migrating cell builds protrusions at the migration site, detaches and adheres to the substrate and moves by force generation by means of the actin cytoskeleton.[50,52] In contrast, the cells in 3D migration have to coordinate and pave their way by sensing nutrition gradients, by proteolysis of extracellular matrix (ECM), or deformation through restricted pores on their path. First, 3D moving cells polarize, build protrusions, and adhere to parts of the ECM (Figure 1.5 a and b). These cancer cells are able to adapt to ECM alterations by their changes of migration mode from the “mesenchymal” type, under available space, to the “amoeboid” type, under limited space conditions (Figure 1.5 c). In addition, the cytoplasm and nucleus have to be deformed and pushed through the

restricted area. Finally, the cell moves forward by actomyosin contraction and de-adhesion and retraction from their back site (Figure 1.5 d and e).[53] Consequently, the cell migration in 3D environment represents a complex machinery, which is, however, more representative for *in vivo* conditions.

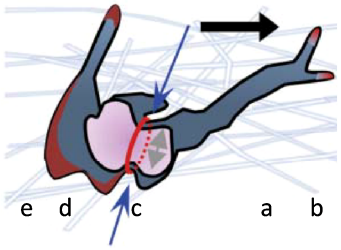

Figure 1.5: Steps of restricted 3D cell migration. Polarization/protrusion (a) and adhesion (b) to extracellular matrix (ECM), deformation of the cytoplasm and the nucleus dependent on physical space through a restricted pore (c, blue arrows with red circle), actomyosin contraction (d) and retraction (e) lead to forward movement of the cell (black arrow).[53]

1.5 Aim of the study

In contrast to microtubule binding drugs, actin binding compounds have not been established in clinical use of cancer treatment, so far. The occurrence of resistance mechanisms and assumed side effects in patients are still limiting the use of actin binding compounds in clinic. However, actin participates in many regulatory cellular processes and therefore represents an attractive target for anti-tumor therapy.

The aim of the study was, to elucidate differentiated effects of actin binding compounds chondramide and miuraenamide on cancer cells beside the prominent actin disruption. For this purpose, the myxobacteria derived compounds should be tested on two major hallmarks of cancer cells: the survival and the migration. Firstly, the impact on cancer cell survival after chondramide treatment in combination with DNA damaging agent doxorubicin, as well as the underlying mechanism should be evaluated. Secondly, we wanted to explore the effects of low dose miuraenamide treatment over a longer period of time on cancer cell migration processes.

In summary, this study aimed to evaluate the pro-apoptotic and anti-metastatic potential of actin binding compounds, beyond simple cytoplasmic actin alterations.

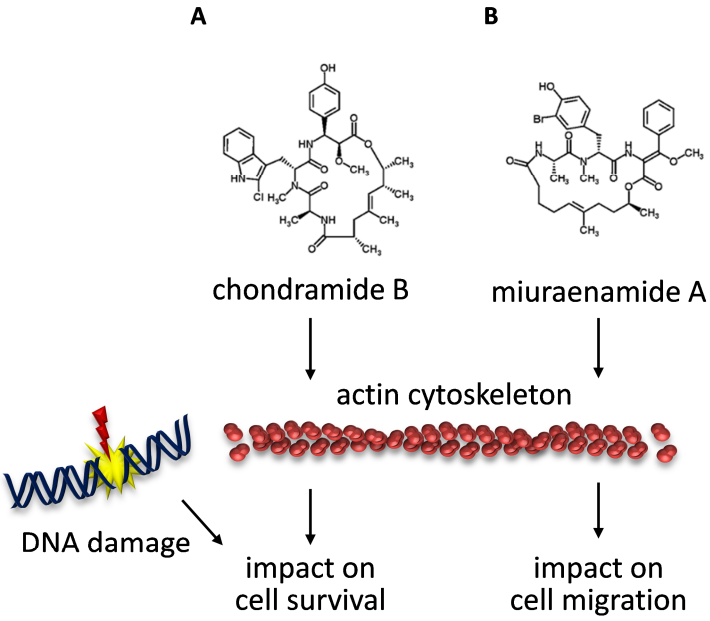

Figure 1.6: Actin binding compounds as a tool for cancer therapy. A: The first aim of the study was to elucidate the effect of chondramide B in combination with the DNA damaging agent doxorubicin concerning DNA damage response mechanism and cancer cell survival pathways. **B:** The second aim of the study was to analyze low dose effects of miuraenamide on the migration of cancer cells.

2 MATERIALS AND METHODS

2.1 Materials

2.1.1 Study compounds

Chondramide B was kindly provided by Prof. Dr. Rolf Mueller, Helmholtz Centre for Infection Research, Saarland University, Saarbruecken, Germany. Miuraenamide A was kindly provided by Prof. Dr. Uli Kazmaier, Institute for Organic Chemistry, Saarland University, Saarbruecken, Germany. Both natural compounds were dissolved in DMSO and stored at -20°C. Doxorubicin, dissolved in H_2O and DNA-PK inhibitor NU7026, dissolved in DMSO, were purchased from Sigma Aldrich, Taufkirchen, Germany.

2.1.2 Chemicals and reagents

The chemicals and reagents were purchased from Sigma Aldrich, Taufkirchen, Germany, unless otherwise listed in the following tables.

Table 2.1: Chemicals and reagents

Reagent	Provider
2,2,2-trichloroethanol	Sigma Aldrich, Taufkirchen, Germany
2,2'-azino-bis(3-ethylbenzothiazoline-6-sulfonic acid)	Sigma-Aldrich, Taufkirchen, Germany
Agarose, low gelling temperature	Sigma Aldrich, Taufkirchen, Germany
Amersham Hybond ECL nitrocellulose membrane	GE Healthcare Europe, Freiburg, Germany
Amersham Hybond P 0.45 PVDF membrane	GE Healthcare Europe, Freiburg, Germany
Amphotericin B	PAA Laboratories, Pasching, Austria
Blotto (non-fat dry milk powder)	Carl Roth, Karlsruhe, Germany

Reagent	Provider
Bovine Serum Albumin (BSA)	Sigma Aldrich, Taufkirchen, Germany
Bradford reagent Roti®-Quant	Carl Roth, Karlsruhe, Germany
Brefeldin A	Sigma Aldrich, Taufkirchen, Germany
CellTiter-Blue®	Promega, Mannheim, Germany
Collagen type I, rat tail	ibidi, Martinsried, Germany
Complete™	Roche diagnostics, Penzberg, Germany
Dimethylsulfoxide (DMSO)	Sigma Aldrich, Taufkirchen, Germany
FluorSave™ Reagent	Millipore, Darmstadt, Germany
FuGENE® HD Transfection Reagent	Promega, Mannheim, Germany
GelRed™ Nucleic Acid Stain	Biotium, Fermont, USA
Hoechst 33342	Sigma Aldrich, Taufkirchen, Germany
Luminol	AppliChem, Darmstadt, Germany
Na_3VO_4	Sigma Aldrich, Taufkirchen, Germany
Page Ruler Prestained Protein Ladder	Fermentas, St. Leon-Rot, Germany
Propidium iodide	Sigma Aldrich, Taufkirchen, Germany
Pyronin Y	AppliChem, Darmstadt, Germany
Pyruvate	PAA Laboratories, Pasching, Austria
Rhodamine-phalloidin	Life Technologies, Darmstadt, Germany
Rotiphorese® Gel 30 (37,5:1)	Carl Roth, Karlsruhe, Germany
Sodium dodecyl sulfate (SDS)	Carl Roth, Karlsruhe, Germany
Tris hydrochloride (Tris HCl)	Sigma Aldrich, Taufkirchen, Germany
Triton® X-100	Millipore, Darmstadt, Germany
Tween® 20	VWR, Darmstadt, Germany
Yo-Pro®-1 Iodide	ThermoFischer Scientific, Germering, Germany

2.1.3 Cell culture reagents

Table 2.2: Cell culture reagents

Cell culture reagent	Producer/Distributor
Boyden chamber	Corning, New York, USA
Collagen G	Biochrom, Berlin, Germany
Dulbecco's modified Eagle's medium (DMEM)	PAN Biotech, Aidenbach, Germany
Endothelial cell growth medium ECGM	Promocell, Heidelberg, Germany
Ethylenediaminetetraacetic acid (EDTA)	Carl Roth, Karlsruhe, Germany
Fetal Calf Serum (FCS)	PAA Laboratories, Pasching, Austria
Glutamine	Sigma Aldrich, Taufkirchen, Germany
McCoy's medium	PAA Laboratories, Pasching, Austria
Penicillin/Streptomycin 100x	PAA Laboratories, Pasching, Austria
RPMI 1640 10x medium	Sigma Aldrich, Taufkirchen, Germany
RPMI 1640 medium	PAN Biotech, Aidenbach, Germany
Trypsin	PAN Biotech, Aidenbach, Germany

2.1.4 Mixtures and kits

Table 2.3: Mixtures and kits

Name	Provider
Dual-Luciferase® Reporter Assay System	Promega, Mannheim, Germany
High-Capacity cDNA Reverse Transcription Kit	Applied Biosystems, Foster City, USA
Qiagen RNeasy® Mini Kit	Qiagen, Hilden, Germany
SYBR® Green PCR Master Mix	ThermoFischer Scientific, Germering, Germany
VECTASTAIN® ABC Kit	Vector Laboratories, Burlingame, USA

2.1.5 Antibodies

Table 2.4: Primary antibodies

Antibody (primary)	Provider
Actin (C4)	Millipore, Darmstadt, Germany
GAPDH (7B)	Santa Cruz Biotechnology, Heidelberg, Germany
GM130 (D6B1)	New England Biolabs, Frankfurt (Main), Germany
Ki67	Abcam, San Francisco, USA
Myo18A	Proteintech Group, Rosemont, USA
NFAT5	ThermoFischer Scientific, Germering, Germany
p300 (NM-1)	ThermoFischer Scientific, Germering, Germany
PARP-1 (Ab-2)	Millipore, Darmstadt, Germany
Phospho-Histone H2A.x (Ser139)	New England Biolabs, Frankfurt (Main), Germany
β-Catenin (H-102)	Santa Cruz Biotechnology, Heidelberg, Germany

Table 2.5: Secondary antibodies

Antibody (secondary)	Provider
Alexa Fluor 488, Goat-Anti-Mouse IgG (H+L)	Molecular Probes, Eugene, USA
Alexa Fluor 488, Goat-Anti-Rabbit IgG (H+L)	Molecular Probes, Eugene, USA
HRP, Goat-Anti-Mouse IgG	Santa Cruz Biotechnology, Heidelberg, Germany
HRP, Goat-Anti-Mouse IgG1	Biozol Diagnostica, Eching, Germany
HRP, Goat-Anti-Rabbit IgG (H+L)	Bio-Rad Laboratories, Munich, Germany
IRDye 680 LT Goat-Anti-Mouse	Li-Cor Biosciences, Bad Homburg, Germany
IRDye 800 Goat-Anti-Mouse IgG (H+L)	Rockland Immunochemicals, Limerick, USA

2.1.6 Cell culture and general lab equipment

Table 2.6: Cell culture and general lab equipment

Name	Provider
Culture flasks, plates	Sarstedt, Nuembrecht, Germany
Eppendorf Safe Lock Tubes	Eppendorf, Hamburg, Germany
FACS tubes	Sarstedt, Nuembrecht, Germany

Name	Provider
Falcons, dishes	TPP, Trasadingen, Switzerland
Haake W19, water bath	Thermo Haake, Karlsruhe, Germany
Heracell™ 150, CO_2 Incubator	ThermoFischer Scientific, Germering, Germany
Herasafe™ KS, biological safety cabinets	ThermoFischer Scientific, Germering, Germany
HLC HBT 130, thermo block	Biometra, Goettingen, Germany
ibidi™ µ-Slide Chemotaxis	ibidi, Munich, Germany
ibidi™ µ-Slide 8 Well	ibidi, Munich, Germany
Mikro 22R, centrifuge	Hettich, Tuttlingen, Germany
NanoDrop 1000 Spectrophotometer	Peqlab, Wilmigton, USA
Orion II Microplate Luminometer	Titertek-Berthold, Pforzheim, Germany
Sunrise™ Microplate Absorbance Reader	Tecan, Maennedorf, Austria
Vi-CELL™ RX Cell Viability Analyzer	Beckman Coulter, Fullerton, USA
VXR Vibrax®, shaker	IKA®-Werke, Staufen, Germany

2.2 Technical equipment

Table 2.7: Technical equipment

Name	Provider
Atomic Force Microscope (AFM) NanoWizard® 4	JPK Instruments, Berlin, Germany
Axiovert 25	Zeiss, Jena, Germany
Canon EOS 450C camera	Canon, Krefeld, Germany
Cantilever MLCT-E/MLCT-C	Bruker AFM Probes, Camarillo, USA
ChemiDoc™ Touch Imaging System	Bio-Rad Laboratories, Munich, Germany
FACSCanto™ II	BD Biosiences, Heidelberg, Germany
Heating system	Okolab, Pozzuoli, Italy
Heating system, multi-well plates	ibidi, Martinsried, Germany
Heating system, universal fit	ibidi, Martinsried, Germany
Inverted microscope Eclipse Ti	Nikon, Duesseldorf, Germany
Leica TCS SP8 SMD	Leica Microsystem, Wetzlar, Germany

Name	Provider
Li-Cor Odyssey® Infrared Imaging System	Li-Cor Biotechnology, Bad Homburg, Germany
LSM 510 Meta	Zeiss, Jena, Germany
Olympus BX41 microscope	Olympus, Center Valley, USA
QuantStudio 3 Real-Time PCR System	ThermoFischer Scientific Germering, Germany

2.3 Cell culture

2.3.1 Cultivation of cell lines

The human mammary carcinoma cell lines MDA-MB-231, SKBR3 and SKOV3 were purchased from Cell Lines Service (Eppelheim, Germany) and were cultivated in DMEM high glucose or RPMI 1640 (in case of SKOV3 cell line) with 1 % penicillin/streptomycin (1.5 mM) and 10 % FCS. The bladder carcinoma cell line T24 was maintained in McCoy's medium supplemented with 1 % penicillin/streptomycin (1.5 mM) and 10 % FCS, and was kindly provided by Dr. Barbara Mayer (Department of Surgery, LMU Munich, Germany) and authenticated by the DSMZ (Braunschweig, Germany). Stable transfected HeLa_ssHRP cells were a kind gift from Dr. von Blume (Max Planck Institute of Biochemistry, Martinsried, Germany) and were cultivated in DMEM high glucose with 1 % penicillin/streptomycin (1.5 mM) and 10 % FCS. HUVECs were purchased from Promocell (Heidelberg, Germany) and maintained in endothelial cell growth medium (ECGM) with 4.7 % supplement mix, 1 % penicillin/streptomycin (1.5 mM), 250 µg/ml amphotericin B and 10 % FCS. All cells were cultivated in an incubator with constant humidity of 37°C and 5 % CO_2. Breast cancer cells were passaged twice or thrice weekly in a ratio of 1:5 to 1:10. Cells were washed with prewarmed PBS and detached with trypsin/EDTA (T/E). Further, cells were resuspended with culture medium and, if necessary counted with Vi-CELL™ RX and seeded in cell culture dishes.

PBS (pH 7.4) NaCl 123.2 mM, Na_2HPO_4 10.4 mM, KH_2PO_4 3.2 mM in H_2O

T/E Trypsin 0.05 %, EDTA 0.2 % in PBS

2.3.2 Freezing and thawing of cells

The cell lines were frozen at -20°C for 1-2 hours afterwards transferred to -80°C overnight (o/n) and stored in cryovials in liquid nitrogen within culture medium supplemented with 20 % FCS, 1 % penicillin/streptomycin and 10 % DMSO. For re-cultivation, they were thawed in 37°C water bath, transferred into 5 ml of warmed media, and seeded into a 25 cm^2 flask. 2-3 days later, the cells were transferred into a 75 cm^2 flask and grown for three days before used for experiments.

2.4 Proliferation and viability

2.4.1 Proliferation assay

Proliferation assay was performed in 96-well plates with a concentration of 5x 10^3 cells/well. Cells were seeded o/n and treated for 72 h with the indicated concentrations of compounds. A few additional seeded wells with untreated cells were measured for day zero control. The cells were fixed and stained, after a washing step with PBS, with crystal violet/methanol. After washing out crystal violet with ethanol/Na-citrate, the absorption was determined by microplate reader at 540 nm.

Crystal violet/methanol	0.5 % crystal violet (w/v), 20 % methanol (v/v)
Ethanol/Na-citrate	50 % ethanol (v/v), 50 % 0.1 M Na-citrat (w/v)

2.4.2 CellTiter-Blue (CTB) viability assay

To analyze the viability of cancer cells, they were seeded in 96-well plates o/n. The cells were treated with the indicated compounds for 72 h or measured for day zero control. The viability of cells was determined by incubation with CellTiter-Blue® (CTB) reagent for 2 h. Measurement was performed with microplate reader.

2.5 Flow cytometry measurement

2.5.1 Propidium iodide (PI) and Yo-Pro-1 (YP) exclusion assay

The cancer cells were cultivated in twelve-well plates with a concentration of $4x\ 10^4$ cells/well, were stimulated with the study compounds and harvested by trypsination in FACS tubes. After a washing step with PBS, the cells were exposed to a solution of propidium iodide (PI, 5 µg/ml) or Yo-Pro-1 (YP, 100 nM) in PBS. Subsequently, cells were analyzed immediately by flow cytometry using FACSCanto™ II.

Dying cells showed increased cell permeability and higher absorption of PI or YP. The fluorescence cytometer showed an increased fluorescence signal at 580 nm (PI) or 509 nm (YP) for dead cells after excited with the 488 nm spectral line of an argon-ion laser. Therefore, cells with a fivefold higher fluorescence signal were considered as PI or YP positive cells.

2.5.2 Nicoletti assay and cell cycle analysis

Cells were cultivated, harvested and washed with PBS as explained in 2.5.1. After the treatment and harvest, cells were exposed to the hypotonic fluorochrome solution (HFS), for 30 min. Next, the DNA of cells was stained with PI by permeabilization with Triton X-100. The percentage of cells in each cell cycle phase could be calculated by a histogram, which depicted the amount of living cells in S, G_1 and G_2 phase peaks. The DNA of dead cells showed fragmentation and could be detected in front of G_1 peak ($subG_1$). The apoptosis rate was calculated by percentage $subG_1$ population.[54]

HFS Triton X-100 0.1 % (v/v), sodium citrate 0.1 % (w/v), propidium iodide 50 µg/ml

2.6 In vivo xenograft mouse model

2.6.1 Animal experiment

$5x\ 10^6$ MDA-MB-231 cells were injected subcutaneously into the flank of each SCID mouse (C.B-17/IcrHan®Hsd-Prkdcscid, Harlan Laboratories, USA). 40 mice were divided into four treatment groups (ten mice per group): solvent (DMSO) control group, two single groups treated intravenously either with doxorubicin (Doxo) 1.5 mg/kg body weight (once a

week) or with chondramide B (ChB) 0.6 mg/kg body weight (thrice a week) and a combination of both. During the treatment the weight of mice was measured and the tumor volume was calculated with the formula $V = a \cdot b^2/2$ every second day. After 36 days the mice were sacrificed and tumor growth and weight were determined. All animal procedures were carried out according to the guidelines of the German law of protection of animal life and approved and controlled by the local ethics committee. The animal experiment was performed by Dr. Rebekka Kubisch and Johanna Busse in the laboratory of Prof. Dr. Ernst Wagner (Pharmaceutical Biotechnology, LMU Munich, Germany).

2.6.2 Histological tumor staining

Tumors were removed, fixed in formalin and embedded in paraffin blocks. Sections were prepared and stained with anti-Ki67 antibody and visualized with the VECTASTAIN® ABC Kit according to the manufacturer's instructions. Four tissues per treatment group were analyzed and images were taken on the Olympus BX41 microscope. The Ki67 positive cells were counted with ImageJ 1.51f and normalized to total number of cells.

2.7 Metastasis assays

2.7.1 Wound healing assay

The wound healing or scratch assay was performed with confluent cell layers. Cells were pretreated for 72 h with the indicated compound concentrations, seeded into 96-well plates and incubated for minimum five hours at 37°C. Scratch was executed with a tip and after 14 h migration cells were stained with crystal violet/methanol. Pictures of the scratch were taken with the Inverted microscope Eclipse Ti.

2.7.2 Boyden chamber assay

With Boyden chamber migration assay the migration through restricted pores towards an FCS gradient could be determined. The cells were pre-stimulated for 72 h with the indicated compound concentration and 2×10^4 cells were seeded without compound in FCS negative medium in the upper compartment of the chamber. The lower

compartment was filled with medium containing 10 % FCS to generate an FCS gradient. After migration of 20 h, cells were fixed and stained with crystal violet/methanol. Remaining cells in the upper compartment were removed with q-tips and pictures of the bottom side of membrane were taken with the Axiovert 25 microscope and Canon EOS 450C camera. The amount of migrated cells was analyzed with ImageJ 1.51f.

2.7.3 Adhesion assay

The adhesion assay was performed with pre-treated cells in 96-well plates. A concentration of 4x 10^4 cells/well were seeded in collagen G coated wells and allowed to adhere for 90 min. Cells were stained with crystal violet/methanol and imaged with Axiovert 25 microscope and adhering cells were counted.

2.7.4 Chemotaxis assay

With the chemotaxis assay, migration of cells along a FCS gradient without environmental restriction could be detected. Cells were pre-treated with the indicated compound concentration and seeded into ibidi^{TM} µ-Slide Chemotaxis, collagen IV coated chamber in compound free medium. After the cells had attached to the chamber slide, the channel was washed with medium without FCS and a gradient was generated by filling one reservoir with FCS negative medium and the other with 10 % FCS medium. For negative control 10 % FCS was filled in both reservoirs, which generates an environment of undirected migration. Images were taken every ten minutes and the indicated migration parameters were calculated by the chemotaxis and migration tool Qt Open Source Edition version 4.3.2.

2.7.5 Three dimensional (3D) collagen I gel migration

Rat tail collagen I gels were prepared according to the manufacturer's protocol. Briefly, gels with a concentration of 2 mg/ml were mixed on ice with 0.25x 10^6 cell/mixture. Collagen I was added at the end and immediately pipetted into ibidi^{TM} µ-Slide Chemotaxis. For gelation, the gel was left 15 min on ice, before incubated for a minimum of 1 h at 37°C, 5 % CO_2 in incubator. The chemotaxis reservoirs were filled with medium

with or without FCS to create an FCS gradient. Life cell images were taken by Inverted microscope Eclipse Ti.

Collagen I gel (150 µl) RPMI 1640 10x (10 µl), NaOH 1 M (3 µl), H_2O (57.2 µl), $NaHCO_3$ 7.5 % (2.5 µl), RPMI 1640 1x (25 µl), Rat tail collagen I 11 mg/ml (27.3 µl), SKOV3 cells 0.25x 10^6 (25 µl)

2.8 HRP secretion assay

HeLa_ssHRP (signal sequence horseradish peroxidase) cells were seeded and pre-stimulated as described before. After an indicated stimulation period, the medium was removed and the cells were washed five times with fresh medium. Further, 300 µl of fresh medium with or without compound were added. Brefeldin A was used as a positive control. The secretion was allowed in an incubator over 4 h, before harvesting the cells. The medium was collected as secretion probe, while cells were trypsinated and collected by centrifugation. The cell pellets were lysed with 0.5 % Triton-X 100 in PBS on ice for 20 min. After an additional centrifugation at 4°C, 14000x g for 20 min, supernatants and pellet fraction were applied to a 96-well plate. The HRP substrate 2,2'-azino-bis(3-ethylbenzothiazoline-6-sulfonic acid) was added to probes and the absorbance was read out at 405 nm with Tecan Microplate Reader. The supernatant signal was normalized to the pellet signal.

2.9 Microscopy

2.9.1 Confocal laser scanning microscopy

The cell lines were seeded in ibidi^{TM} µ-Slides, cultivated o/n and treated with different compounds for indicated time points. The cells were permeabilized with Triton X-100 0.1 % (v/v), blocked with BSA 1 % or 5 % and stained first with a specific primary antibody (Table 2.8). The primary antibodies were diluted 1:400 or 1:500 with BSA 1 % and incubated for 1 h at RT or o/n at 4°C. After two washing steps with PBS^+, secondary fluorescence antibodies (Table 2.9), diluted 1:1000 in BSA 1 %, were incubated at RT for 1 h. The fluorescence signal was optimized by sealing cells with mounting medium FluorSave^{TM} reagent and a cover slip.

PBS^{+} Ca^{2+}/Mg^{2+} (pH 7.4)	NaCl 136.9 mM, KCl 2.7 mM, Na_2HPO_4 8.1 mM, KH_2PO_4 3.2 mM, $CaCl_2$ x $2H_2O$ 0.7 mM, $MgCl_2$ x $6H_2O$ 0.5 mM

Table 2.8: Primary antibody for fluorescence staining

Antigen	Source	Dilution
GM130 (D6B1)	Rabbit	1:500
Myo18A	Rabbit	1:400
NFAT5	Mouse	1:500
β-Catenin (H-102)	Rabbit	1:500
p300	Mouse	1:400

Table 2.9: Secondary antibody for fluorescence staining

Fluorescence labeled Antibody	Dilution
Alexa Fluor 488, Goat-Anti-Rabbit IgG (H+L)	1:1000
Alexa Fluor 488, Goat-Anti-Mouse IgG (H+L)	1:1000

2.9.2 Life cell imaging

The Inverted microscope Eclipse Ti was used for the imaging of migrating cells during life cell experiments. Pictures were obtained using the 10x phase contrast objective and charge coupled device camera every ten minutes over 20 h. The slide was incubated at 37°C, 5 % CO_2, humidity of 80 % during measurements. Images were evaluated with ImageJ 1.51f.

2.9.3 Atomic force microscopy

Cells were seeded into 34 mm dishes and stimulated for 72 h with the indicated concentrations of compound. The stiffness of total cell surface and the specific nucleus stiffness was measured with the atomic force microscope (AFM) NanoWizard® 4 and subsequently analyzed by Daniel Ruediger. Briefly, cantilevers (MLCT-E: k=0.1 N/m, f=38 kHz; MLCT-C: k=0.01 N/m; f=7 kHz; silicon nitride; front angle 15±2.5°; quadratic pyramid tip shape) were calibrated with contact-free method and used for measurements in the contact mode. Total cellular stiffness was determined by a force map with an area of 80x80 µm, whereas, stiffness of the nucleus was measured by single force curves. For both measurements the velocity was 2 µm/s and the set point was appointed to 1 nN.

The data were analyzed with the NanoWizard® Data Processing software version 6.0.50 and the stiffness was calculated according the Hertzian contact model (young's modulus).

2.10 DNA damage response measurements

2.10.1 Comet assay

SKOV3 cells were seeded and treated as described before. 20 µl cells were trypsinated and mixed with 20 µl 37°C prewarmed 1.4 % agarose, low gelling temperature with GelRed™ to an agarose concentration of 0.7 %. 30 µl of cell-agarose mix were pipetted on pre-coated glass slides and solidified on ice for 10 min. The slides were lysed in lysis buffer o/n at 4°C or 2 h in the dark. Afterwards, the slides were washed with PBS and transferred to the electrophoresis tank filled with electrophoresis buffer. Further, the electrophoresis was proceeded 10 min at 300 mA (25-30 V). The slides were washed again with PBS and incubated in 70 % ethanol for 1 h and further air-dried o/n at RT. The images were taken with a confocal microscope after covering the slides with FluorSave™ and a cover slip. Tail moment (T_M) was quantified with the ImageJ 1.51f plugin OpenComet 1.3 with the following formula: T_M = tail length x tail DNA %.

Lysis buffer NaCl 2.5 M, EDTA 0.1 M, Tris 10 mM, Triton X-100 1 %, pH 10 in H_2O

Electrophoresis buffer NaCl 0.3 M, EDTA 1 mM, pH 13 in H_2O

2.10.2 Golgi area

SKOV3 cells were seeded and treated as described for confocal laser scanning microscopy in ibidi™ µ-Slides. Cells were stained with GM130 antibody (1:400 in 5 % BSA), fixed and imaged with an LSM 510 Meta microscope. The Golgi area was analyzed by calculation of Golgi signal normalized to the cell number with ImageJ 1.51f.

2.11 Quantitative real-time PCR analysis

Cells were cultivated in six-well plates and stimulated as described before. Total mRNA was isolated by Qiagen RNeasy® Mini Kit according to the manufacturer's protocol. mRNA level was determined with the NanoDrop 1000 Spectrophotometer and 1.5 to 2.0 µg

mRNA were transcribed into complementary DNA (cDNA) by High-Capacity cDNA reverse transcriptase. Quantitative real-time PCR was performed in QuantStudio 3 Real-Time PCR System with SYBR® Green Master Mix, indicated forward and reverse primer, and template cDNA. GAPDH was used as housekeeping gene. All primers were purchased from Metabion, Planegg, Germany.

Table 2.10: qRT-PCR primer

mRNA	Forward	Reverse
GAPDH	5'-ACG GGA AGC TTG TCA TCA AT-3'	5'-CAT CGC CCC ACT TGA TTT T-3'
EP300	5'-CAT GGG TAT GAA CCC ACC TC-3'	5'-GTG GAG CCA TGT TCA AAG GT-3'
CYR61	5'-ACC CTT CTC CAC TTG ACC AG-3'	5'-CTT GGC GCA GAC CTT ACA G-3'

2.12 Western blot

Western blot analysis was performed to determine protein levels of whole cell lysates or cell fractions. The cells were cultivated as described in 2.3.1 and stimulated with compounds for the indicated time points.

2.12.1 Total cell lysate

The detached cells from three wells were pooled in culture medium and centrifuged for 10 min at 1500 rpm at 4°C. The supernatant was discarded and cells were washed with 500 µl PBS and transferred to Eppendorf tubes. After additional centrifugation the supernatant was again discarded and 85 µl of lysis buffer were added. Samples were frozen o/n at -20°C and further centrifuged again at 10000x g, 4°C for 10 min. 80 µl of supernatant (cell lysates) were collected for SDS PAGE with 20 µl 5x sample buffer and boiled 95°C for 5 min. 5 µl of supernatant were diluted with 45 µl distilled water and were used for Bradford protein quantification. Protein amounts were determined with Roti®-Quant as described before by Bradford.[55] 10 µl of diluted lysates or BSA standard stock solution and 190 µl of 1x Bradford solutions were pipetted in a flat-bottom 96-well plate. Samples were incubated with Bradford reagent and measured in ELISA reader. Concentration of samples was adapted with 1x SDS sample buffer. SDS gels were prepared for separating gel with a concentration of 7.5 % to 12 % and stacking gel in glass

plates. After polymerization, gels were stored at 8°C. For the electrophoresis, 20-30 ng of protein samples and diluted Page Ruler were loaded on the prepared gel. The chamber was filled with Epho buffer and the following running program was adjusted: P1.1: 100 V, 500 mA, 150 W for 21 min and P1.2: 200 V, 500 mA, 150 W for 38 min. Usually, stain-free gels were prepared. Herein, the tryptophan in proteins undergo a reaction by UV light exposure and displayed visualizable fluorescence signal, therefore, total protein amount could be detected.[56] The proteins were transferred in 1 h 20 min from the gel to a nitrocellulose or PVDF membrane, which were activated in tank buffer. Afterwards, the membrane was blocked with 5 % BSA in TBS-T for 1 h at RT. Finally, the proteins on the membranes were incubated with primary antibody o/n at 4°C with the following solutions:

Table 2.11: Dilution of primary antibody

Antigen	Source	Dilution	Solvents
Actin (C4)	Mouse IgG1	1:1000	Blotto 1 %
GAPDH (7B)	Mouse	1:1000	Blotto 1 %
p300 (NM-1)	Mouse IgG1	1:1000	BSA 5 %
PARP-1 (Ab-2)	Mouse IgG1	1:1000	BSA 5 %
phospho-Histone H2A.x (Ser139)	Rabbit	1:1000	BSA 5 %
Myo18A	Rabbit	1:1000	BSA 5 %

The membranes were incubated with secondary HRP-conjugated antibodies or Li-Cor fluorescence antibodies after three washing steps with TBS-T for 1 h at RT. The following antibody solutions were used:

Table 2.12: Dilution of secondary antibody

Secondary Antibody	Dilution	Solvents
HRP, Goat-Anti-Mouse IgG	1:10000	BSA 1 %
HRP, Goat-Anti-Mouse IgG1	1:10000	BSA 1 %
HRP, Goat-Anti-Rabbit IgG (H+L)	1:10000	BSA 1 %
IRDye 680 LT Goat-Anti-Mouse	1:10000	Blotto 1 %
IRDye 800 Goat-Anti-Mouse IgG (H+L)	1:10000	Blotto 1 %

The membranes were incubated either with HRP Homemade ECL solution, which activated the turnover of luminol by HRP and lead to a detectable chemiluminescence

signal by ChemiDoc™ Touch Imaging System, or were directly measured with Li-Cor Odyssey® Infrared Imaging System, if incubated with the IRDye antibodies. The band intensity of detected Western blot was normalized to the total protein amount (stain-free) or GAPDH as loading control.

Phospho-lysis buffer	NaCl 137 mM, Glycerol 10 %, $Na_4P_2O_7$ x $10H_2O$ 2 mM, Na_2EDTA 2 mM, Tris-Base 20 mM, Triton-X 100 1 %, Na_2-glycerophosphate x $5H_2O$ 20 mM, NaF 10 mM, PMSF 1 mM, Complete™ 25x 4 %, Na_3VO_4 2 mM
5x SDS sample buffer	Tris HCl (pH 6.8) 3.13 M, Glycerol 10 %, SDS 20 %, DTT 16 %, Pyronin Y 5 % in H_2O; 1x SDS sample buffer were diluted in H_2O
Separating gel	30 % Rotiphorese® 5 ml, Tris HCl 1.5 M (pH 8.8) 3.75 ml, SDS 10 % 150 µl, H_2O 6.1 ml, 0.5 % 2,2,2-trichloroethanol, TEMED 15 µl, APS 10 % 75 µl
Stacking gel	30 % Rotiphorese® 1.275 ml, Tris HCl 1.25 M (pH 6.8) 750 µl, SDS 10 % 75 µl, H_2O 5.25 ml, TEMED 15 µl, APS 10 % 75 µl
5x Electrophoresis buffer (Epho)	Tris-base 24.8 mM, Glycine 191.8 mM, SDS 3.5 mM in H_2O; 1x Epho diluted 1:5 in H_2O
5x Tank buffer	Tris-base 25 mM, Glycine 192 mM in H_2O
TBS-T (pH 8.0)	Tris HCl 24.8 mM, NaCl 190 mM, Tween 20 0.2 % in H_2O
HRP Homemade ECL	Luminol 1.25 mM, Cumaric acid 0.2 mM, Tris-base HCl (pH 8.5) 0.1 M, H_2O_2 0.009 % in H_2O

2.12.2 Cytosolic-cytoskeletal fractionation

The cytosolic-cytoskeletal fractionation was modified according to Zeidman *et al*.[57] Cells were centrifuged after trypsination at 1500 rpm for 10 min, 4°C. Supernatant was discarded and the cells were lysed for 30 min with phospho-lysis buffer (see 2.12.1) supplemented with iodoacetic acid 4 mM. The cells were centrifuged at 300x g to pelletize debris and nuclei. Supernatant was further centrifuged at 14000 rpm, which collected the cytoskeletal fraction as pellet and the cytosolic fraction in supernatant. Cytoskeletal fraction was collected in PBS supplemented with PMSF (1 mM), Na_3VO_4 (2 mM), Complete™ (25x 1 %) and iodoacetic acid (4 mM). Bradford protein quantification and the protein detection were performed as described in 2.12.1.

2.13 Reporter gene assay

Cells were seeded in 24-well plates and transfected five hours later with reporter gene plasmid M50 Super 8x TOPFlash or M51 Super 8x FOPFlash (TOPFlash mutant) (#12456 and #12457, Addgene, Cambridge, USA) and one-tenth of pGL4.74[hRluc/TK] plasmid (Promega, Mannheim, Germany) for 72 h. The day after transfection cells were stimulated with compound. LiCl (40 mM) was used for TCF/Lef1 promoter activation by disinhibiting β-catenin. The luciferase intensity was measured 56 h after treatment with Promega Dual-Luciferase kit according to manufacturer's protocol. Briefly, cells were washed with PBS, lysed with 50 µl of 1x passive lysis buffer (Promega kit), and plates were frozen o/n at -80°C. 20 µl of the lysed unfrozen cells were transferred to luminometer plates. 100 µl Luciferase Assay Reagent II (Promega kit) were added in each well to measure the firefly luciferase activity and afterwards 100 µl Stop & Glo (Promega kit) reagent were added to stop the firefly luciferase activity and measure the activity of renilla luciferase. The chemiluminescence signal was determined using the Orion II Microplate Luminometer.

2.14 Calculations and statistics

2.14.1 Calculation of specific cell death and Bliss synergism

Specific cell death (and apoptosis) was calculated by the following formula:

$$spec.\,cell\ death = \frac{cell\ death\ [\%, comp] - cell\ death\ [\%, Ctrl]}{100 - cell\ death\ [\%, Ctrl])} * 100$$

Formula 2.1: Calculation of specific cell death (spec. cell death). comp: compound, Ctrl: control.[58]

Synergy effect of compounds was calculated by using the formula of Bliss synergism. The value of Bliss synergism was calculated as following:

$$Value = \frac{C[combi\ treat]}{(C[comp\ A] + C[comp\ B]) - (C[comp\ A] * C[comp\ B])}$$

Formula 2.2: Calculation of Bliss synergism. C: cytotoxic fraction, combi treat: combination treatment, comp: compound.[59]

Values > 1.05 indicated Bliss synergism, values from 0.95 to 1.05 indicated additivity and values < 0.95 indicated Bliss antagonism.

2.14.2 Proteome data

The proteome data was analyzed using Perseus MaxQuant software. The detected proteins were grouped into ten clusters. The cluster with down-regulated proteins after stimulation for 56 h was depicted in a plot with the statistic software R (R version 3.3.2). GOBPs (Gene Ontology and Biological Pathways) and KEGG (Kyoto Encyclopedia of Genes and Genomes) pathways were plotted with a threshold of FDR < 0.5.[60] Pathway with FDR < 0.2 (plotted in orange) and the highest enrichment values (enrichment > 2) were depicted in red with annotations.

2.14.3 Statistics

The experiments were done in triplicates and performed three times, if not otherwise noted. One-way ANOVA test with relevant posttest (Dunnett's Multiple Comparisons or Bonferroni's Multiple Comparison Test) or paired two tailed t-test were used to assess the significance between treatment groups or pairs. The statistical analysis was conducted with GraphPad Prism 5 and Microsoft Excel.

3 RESULTS

3.1 Targeting the DNA damage response in cancer via the actin cytoskeleton

Actin binding agents were supposed to induce strong side effects in application of higher dosage. The combination of compounds such as chondramide B (ChB) with common chemotherapeutics could circumvent such limiting factors. For instance, the DNA damaging agent doxorubicin (Doxo) was used for decades in the clinic in combination or triple therapy.[8]

3.1.1 Combination of doxorubicin and chondramide B reduced tumor growth *in vivo*

Based on this knowledge and on preliminary results of my master thesis, a xenograft *in vivo* trial with immunodeficient SCID mice was performed in order to elucidate the impact of Doxo and ChB combination treatment on tumor formation. The animal experiment was conducted as described in 2.6.

The combination treatment of mice inhibited growth of MDA-MB-231 tumors after 36 days (Figure 3.1 A). Here, the tumor volume of single or control treated mice was 211 to 242 mm^3, whereas the combination treated group showed a reduction by half of the tumor volume to about 122 mm^3. Further, the number of Ki67 positive cells in tumor sections (Figure 3.1 B) was decreased in the combination treatment (9 %) in comparison to control and ChB (29 %). Those results indicated an inhibition of proliferation of combination treated tumors in mice. The observed health conditions of combination treated mice, represented by the body weight (Figure 3.1 C), were unaffected by combination treatment of ChB and Doxo and showed conditions comparable to the control group. In summary, the combination treatment achieved growth inhibitory effects on xenograft tumors and was well tolerated by tested mice.

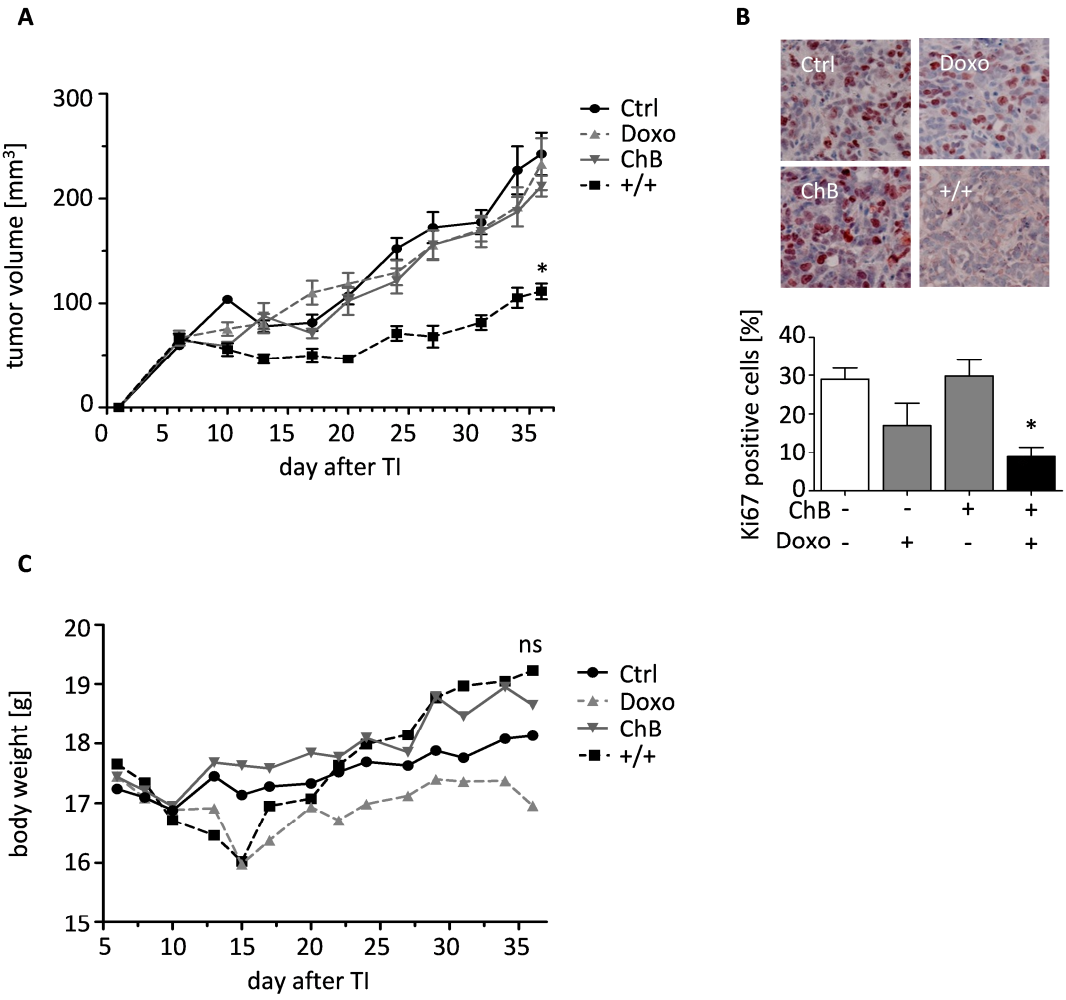

Figure 3.1: Combination treatment (+/+) of doxorubicin (Doxo) and chondramide B (ChB) was tolerable and inhibited tumor growth and proliferation *in vivo*. MDA-MB-231 cells were ectopically injected into in the flank of SCID mice. DMSO was used as solvent control (Ctrl); doxorubicin (Doxo) 3.5 mg/kg body weight (once a week), chondramide (ChB) 0.6 mg/kg body weight (thrice a week) and a combination of ChB and Doxo. **A:** 8-10 mice per group were treated with single, combination or solvent. **B:** Proliferation marker Ki67 (red) staining of paraffin embedded tumor sections. One representative staining per treatment group is shown with a 40x magnification and quantification, n=4. **C:** Progression of body weight over the treatment, n=8-19. TI, tumor injection. One-Way ANOVA/Bonferroni's Multiple Comparison Test, *$p < 0.05$.

3.1.2 Cell death was induced in different cancer cell lines

In line with the *in vivo* experiment, we were interested to elucidate the exact mechanism behind this prominent combination treatment effect of inhibiting tumor growth (Figure 3.1). Therefore, *in vitro* experiments with different cell lines were conducted. First, we tested different concentrations of chondramide (ChB) and doxorubicin (Doxo) in CTB viability assays, and observed the highest reduction of viability with the combination of Doxo 250 nM and ChB 75 nM or 100 nM, with concurrent effects by ChB single treatment. Furthermore, the specific cell death and apoptosis induction after combination treatment with ChB and Doxo were analyzed. The amount of dying cells was determined dependent on the cell line by YP exclusion or Nicoletti assay. Figure 3.2 depicts the significantly increased induction of specific cell death in MDA-MB-231 cells (B) and specific apoptosis of T24 cells (C) in combination treatment of ChB and Doxo. Additionally, the PARP-1 cleavage was significantly increased after the combination treatment (D). The tested compounds, ChB and Doxo, demonstrated synergistic effects in combination treatment indicated by the Bliss value of 1.56 for MDA-MB-231 and 1.82 for T24 cells on cell death induction. These results pointed out the reproducibility of the synergistic effects *in vitro* of actin binding compound ChB and DNA damaging agent Doxo.

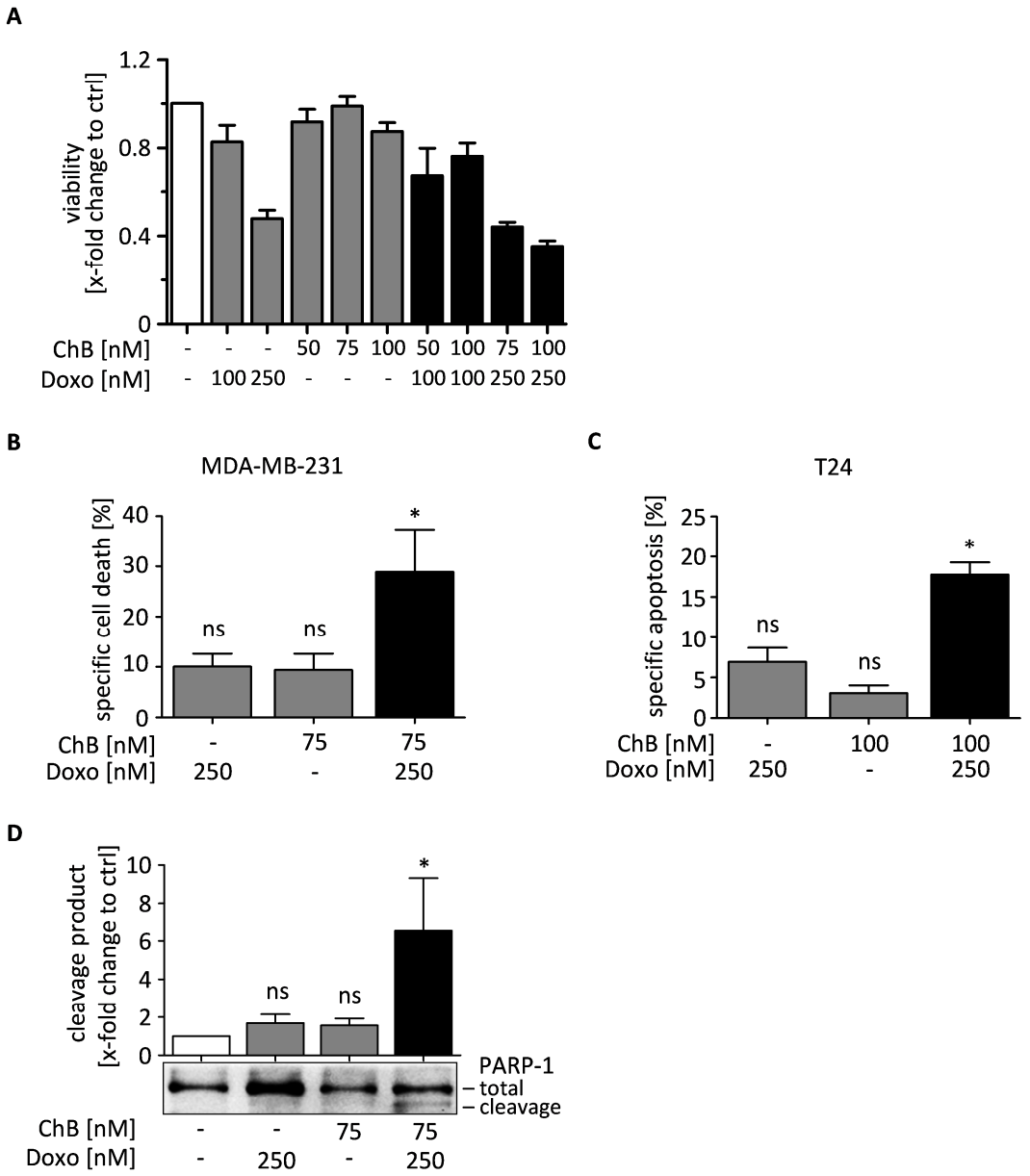

Figure 3.2: Viability, cell death and apoptosis induction after 72 h (T24) and 48 h (MDA-MB-231) combination treatment with chondramide B (ChB) and doxorubicin (Doxo). A: CTB viability assay after 72 h treatment with the indicated concentrations of ChB and Doxo, n=3-4. **B and C:** Specific cell death and apoptosis analysis of MDA-MB-231 and T24 cells. **D:** Western blot analysis of apoptosis markers PARP-1 in MDA-MB-231 normalized to total protein amount (stain-free), n=3. ns, not significant. One-Way ANOVA/Bonferroni's Multiple Comparison Test, *p < 0.05,

3.1.3 The combination treatment increased DNA damage

Following the confirmation of functional effects *in vivo* and *in vitro*, we were interested in the synergistic mode of action of both compounds. Doxo induces DNA double strand breaks and is known for its DNA damaging properties, while a link between actin binding agents such as ChB and DNA damage repair mechanisms has not been clarified yet. To evaluate the synergistic effects of ChB and Doxo, the amount of phosphorylation of histone 2A.x (γH2A.x), which is recruited to the DNA double strand breaks, was tested (Figure 3.3 A). γH2A.x was increased in Doxo single treated cells, but even more after the combination with ChB. The treatment with ChB showed no phosphorylated H2A.x. Aside from increased γH2A.x amounts the Comet assay was performed. Thus, the DNA double strand break induction due to combination treatment was analyzed (Figure 3.3 B). The DNA damage was significantly increased by ChB and Doxo treatment to 1.7-fold as compared with Doxo single treatment, indicated by higher values of tail moment.

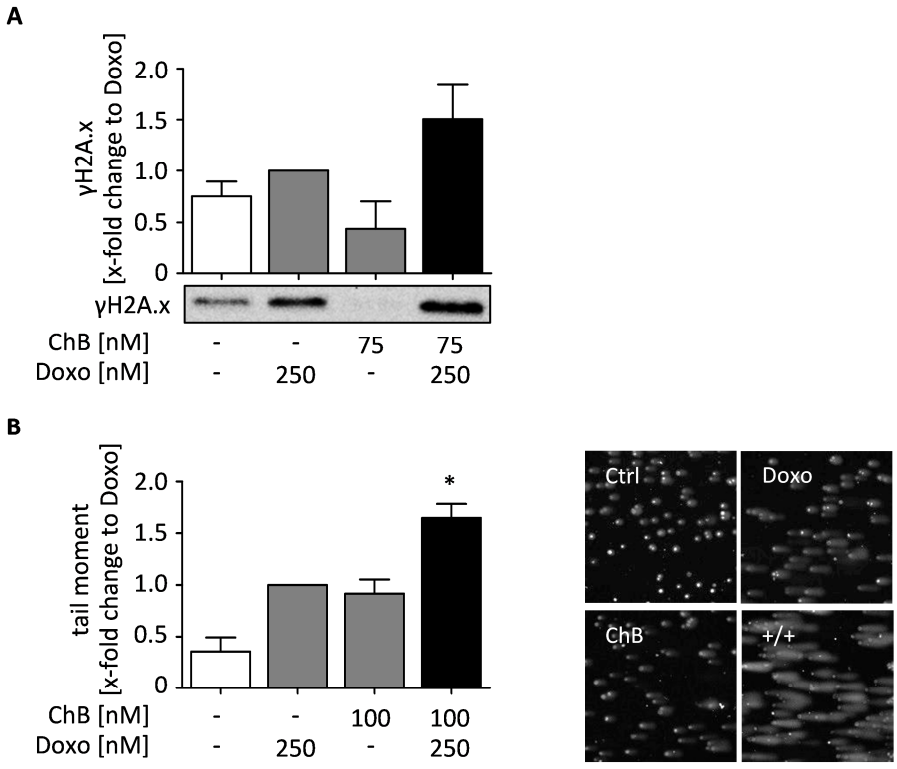

Figure 3.3: The combination treatment in cancer cell lines showed increased DNA damage. Cells were treated for 3 h with the indicated concentrations of chondramide B (ChB) and doxorubicin (Doxo). **A:** Western blot analysis and the quantification of DNA damage marker γH2A.x in treated MDA-MB-231 cells. **B:** Detection of DNA double strand breaks in treated T24 cells with Comet assay. The quantification of tail moment and one representative image per treatment is shown with a magnification of 20x, n=3. ns, not significant. One-Way ANOVA/Bonferroni's Multiple Comparison Test, *$p < 0.05$.

3.1.4 DNA damage induced Golgi dispersal was altered after ChB treatment

In 2014, Farber-Katz *et al.* published the connection of DNA damage response (DDR) mechanism and alteration of Golgi complex.[43] As they stated the dispersal of Golgi complex as a significant response to DNA damage, we measured the Golgi area after Doxo and ChB single and in combination treatment. The confocal microscopy staining of Doxo single treated MDA-MB-231 cells showed significantly increased Golgi area up to 2.5-fold change to control (Figure 3.4). The combination treatment with ChB displayed a reduction of Golgi area comparable to the control or ChB single treatment, which suggested no considerable DDR induction (Figure 3.4). This result indicated the inhibition of DNA damage repair response by ChB after DNA damage induction by Doxo.

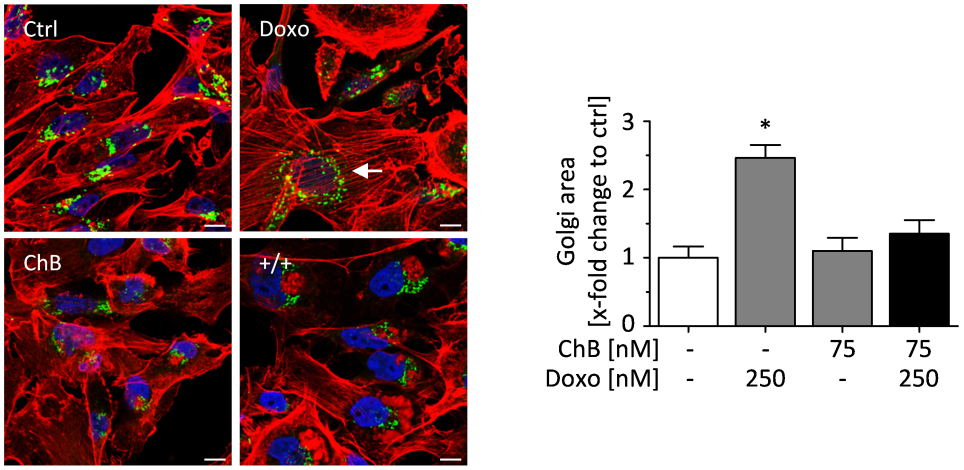

Figure 3.4: The combination treatment showed interrupted Golgi dispersal. Immunostaining of MDA-MB-231 cells treated with chondramide B (ChB), doxorubicin (Doxo) or a combination of both compounds for 48 h. Stained for Golgi complex (GM130, green), actin (rhodamine-phalloidin, red) and nucleus (Hoechst 33342, blue) and the quantification of Golgi area. One representative image per treatment is shown, n=3. White bars indicate 10 µm. One-Way ANOVA/Bonferroni's Multiple Comparison Test, *$p < 0.05$.

3.1.5 ChB interrupted the signaling cascade by myosin 18A trapping

The unconventional myosin 18A (Myo18A) is important for the Golgi dependent DNA damage response (DDR) followed by increased survival.[43] Concurrently, the actin polymerizing compound, ChB, is known to induce actin agglomerates and was verified to trap and thus, to inhibit the function of pro-survival proteins.[33] Therefore the localization of Myo18A relating to actin agglomerates was determined (Figure 3.5). The confocal microscopy pictures displayed a prominent co-localization of Myo18A in actin agglomerates after ChB single treatment and in the combination with Doxo (Figure 3.5 A). Furthermore, the cytosolic-cytoskeletal fractionation depicted enhanced Myo18A protein amount simultaneously with actin in the cytoskeletal fraction (Figure 3.5 B). Those results indicated the inhibition of Golgi dispersal via Myo18A trapping due to the induction of actin agglomerates.

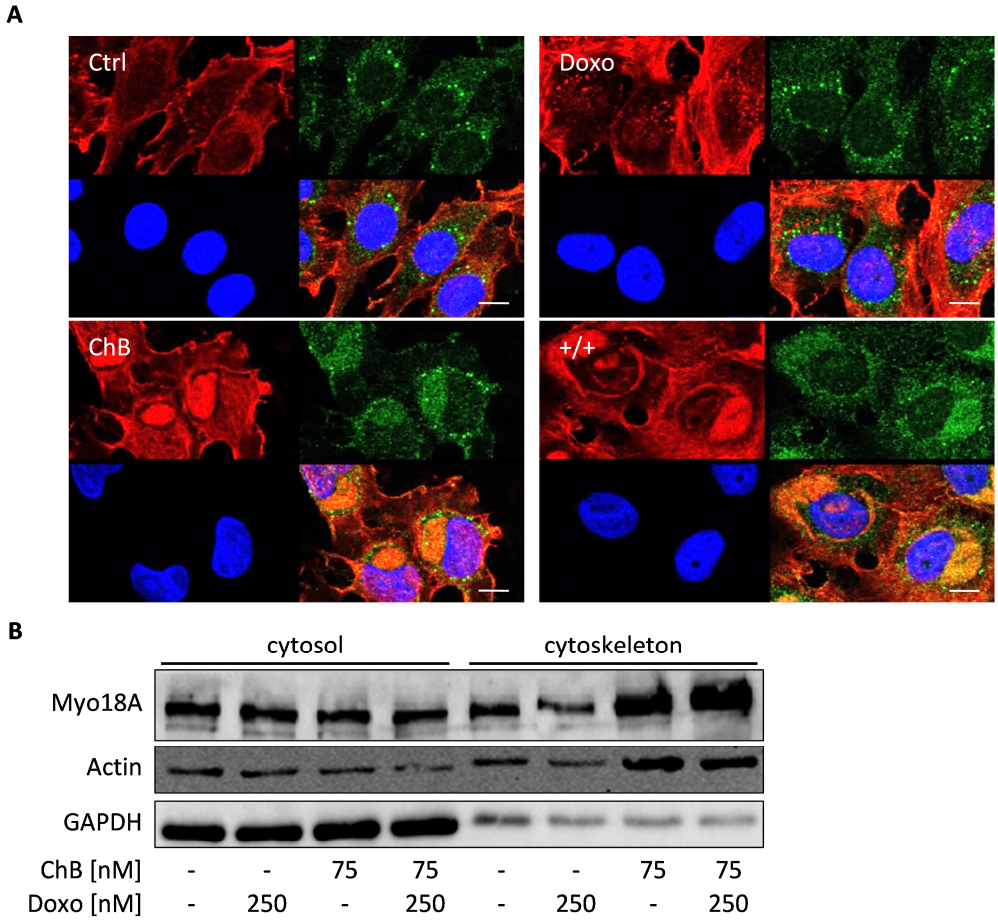

Figure 3.5: Combination treatment showed trapping of myosin 18A (Myo18A) in actin agglomerates. T24 cells were treated with the indicated concentrations of chondramide B (ChB) and doxorubicin (Doxo). **A:** Immunostaining after 48 h treatment of T24 stained for Myo18A (antibody, green), actin (rhodamine-phalloidin, red) and nucleus (Hoechst 33342, blue)**,** n=3. **B:** Western blot analysis of the cytosolic-cytoskeletal fractionation of T24 cells after 6 h treatment, n=1. One representative image per treatment is shown. White bars indicate 10 µm.

3.1.6 DNA-PK was crucial for Golgi dispersal cascade and cell survival

DNA-PK is one of the numerous DNA damage activated protein kinases and turned out to phosphorylate GOLPH3 followed by Golgi dispersal due to its kinase activity.[43] According to the results of Farber-Katz *et al.*, DNA-PK activity was inhibited by the specific inhibitor NU7026. The combination treatment of NU7026 and Doxo showed an inhibition of Golgi dispersal due to the suppression of DDR cascade (Figure 3.6 A). Moreover, the inhibition of Golgi dispersal by suppression of DNA-PK indicated the induction of cell death after DNA damage triggered by Doxo (Figure 3.6 B). This specific cell death induction showed a comparable Bliss synergism value of 1.56 by combination treatment of Doxo and NU7026. Based on these results, it could be concluded that the inhibition of DNA-PK activity

indicated the same functional outcome as trapping of Myo18A via actin agglomerates after ChB treatment and ended in the induction of cell death in the cancer cell line MDA-MB-231.

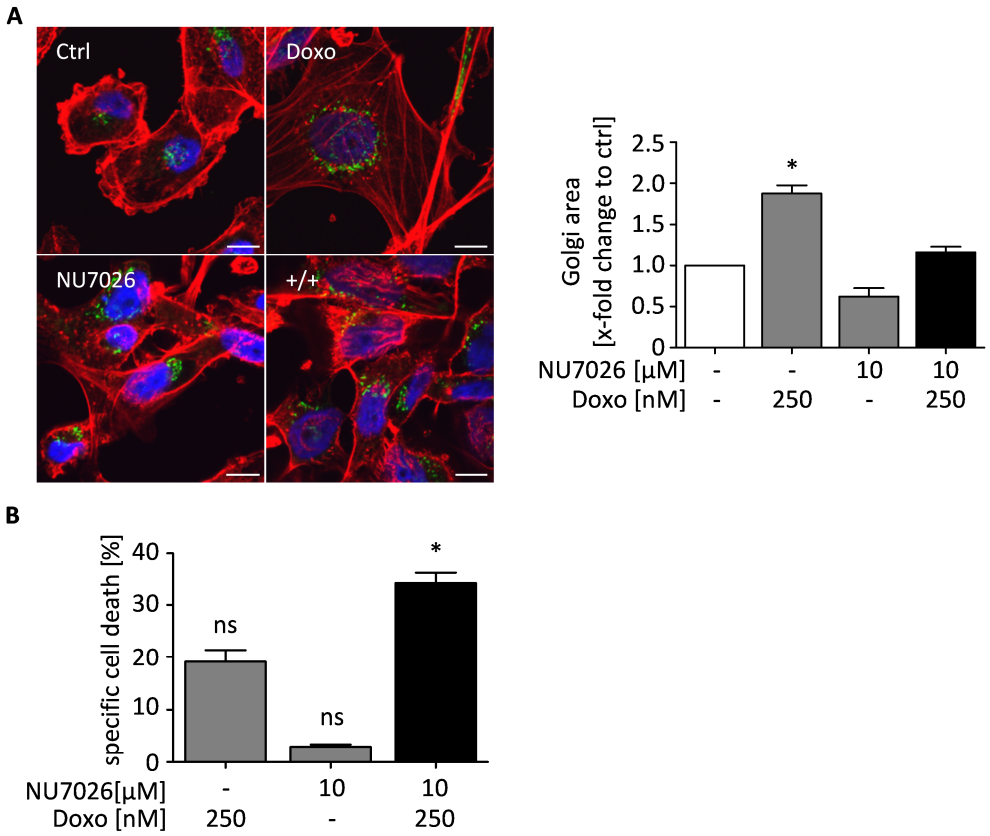

Figure 3.6: NU7026 inhibited the Golgi dispersal and induced cell death in combination with Doxo. MDA-MB-231 cells were treated for 48 h with the indicated concentrations of NU7026 and doxorubicin (Doxo). **A:** Stained for Golgi complex (GM130, green), actin (rhodamine-phalloidin, red), and nucleus (Hoechst 33342, blue) with the quantification of Golgi area (bar diagram). One representative image per treatment is shown, n=3. **B:** Specific cell death analysis, n=3. White bars indicate 10 µm. One-Way ANOVA/Bonferroni's Multiple Comparison Test, *p < 0.05.

3.1.7 SKBR3 cells were insensitive to combination treatment

The examination of another cancer cell line validated the importance of Golgi response after DNA damage. The SKBR3 cell line depicted an altered Golgi localization in control cells compared to MDA-MB-231 cells. In control cells the Golgi complex was more spread around the nucleus and showed no enhanced Golgi area after Doxo treatment although the DNA was damaged even in a lower Doxo concentration, as assessed by the DNA damage indicator γH2A.x (Figure 3.7 A and B). Furthermore, DNA damage was not increased after combination treatment of ChB and Doxo in SKBR3 cells and showed no enhanced cell death induction (Figure 3.7 C). These data suggested the importance of

DNA response mechanism based on Golgi dispersal. The synergistic effects of Doxo and ChB need the DDR dependent on Golgi dispersal, as it was the case in MDA-MB-231 cells and T24 (Figure 3.2, Figure 3.4), to induce higher DNA damage followed by the induction of cell death.

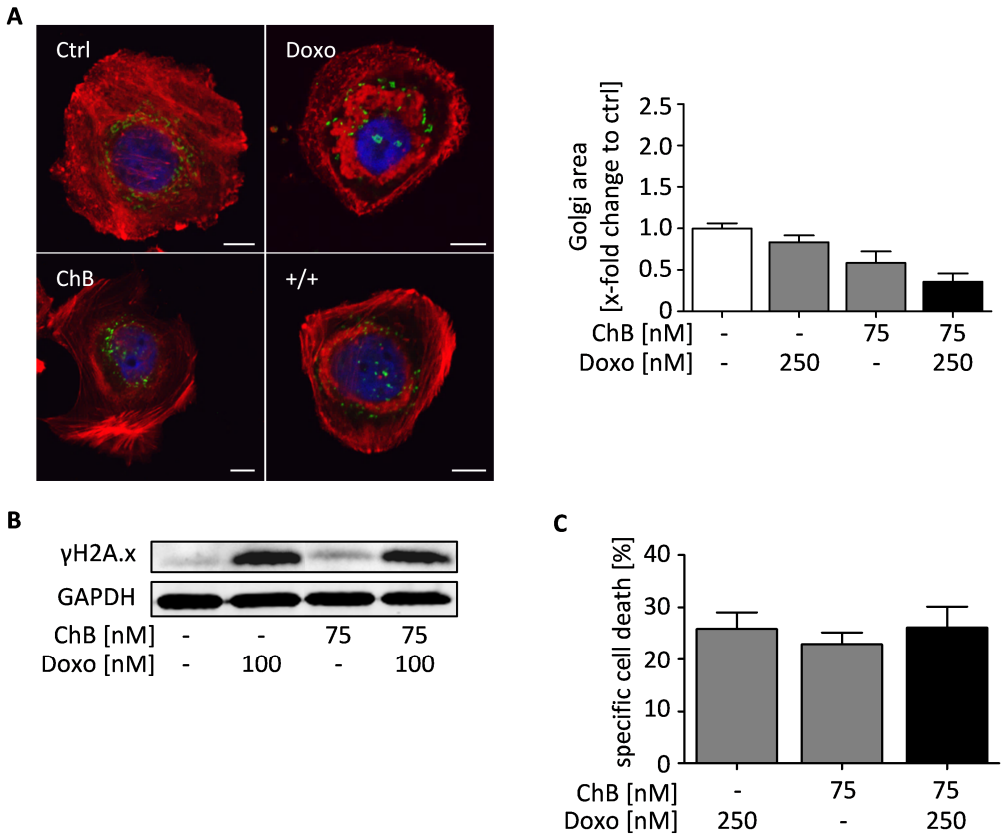

Figure 3.7: SKBR3 cells showed no induction of cell death due to altered Golgi response. SKBR3 cells were treated for 48 h with the indicated concentrations of chondramide B (ChB) and doxorubicin (Doxo). **A:** Stained for Golgi complex (GM130, green), actin (rhodamine-phalloidin, red), and nucleus (Hoechst 33342, blue) and the quantification of Golgi area (bar diagram). One representative image per treatment is shown, n=3. **B:** Western blot analysis of DNA damage marker γH2A.x and loading control GAPDH. **C:** Specific cell death analysis, n=3. White bars indicate 10 µm. Golgi dispersal images with SKBR3 and the quantification were conducted by Alisa Krieg.

3.1.8 Combination treatment showed low toxicity levels on non-cancer cells

As mentioned, the side effects induced by Doxo treatment are known to be very prominent. Especially the cardiotoxicity limits the clinical use of Doxo, and combination compounds with non-additive cardiac effects are needed.[49] Therefore, the effect of ChB and Doxo was tested in neonatal rat cardiomyocytes (Figure 3.8 A and B). The number of cardiomyocytes after combination treatment was still higher (0.48-fold) in comparison to the standard *in vitro* dose of 1000 nM Doxo (0.13-fold), which indicated lower cardiotoxicity. In line, the hypertrophy of cardiomyocytes was determined by the cardiomyocyte area measured with an α-actinin staining. The treatment of ChB and Doxo showed no significantly enhanced cardiomyocyte area and pointed out the negligible side effects of the combination treatment. The second examined non-cancer cell type was the human umbilical vein endothelial cell (Figure 3.8 C). The investigation of endothelial cells showed no induction of apoptosis and underlines a high feasibility of the combination treatment for future clinical trials.

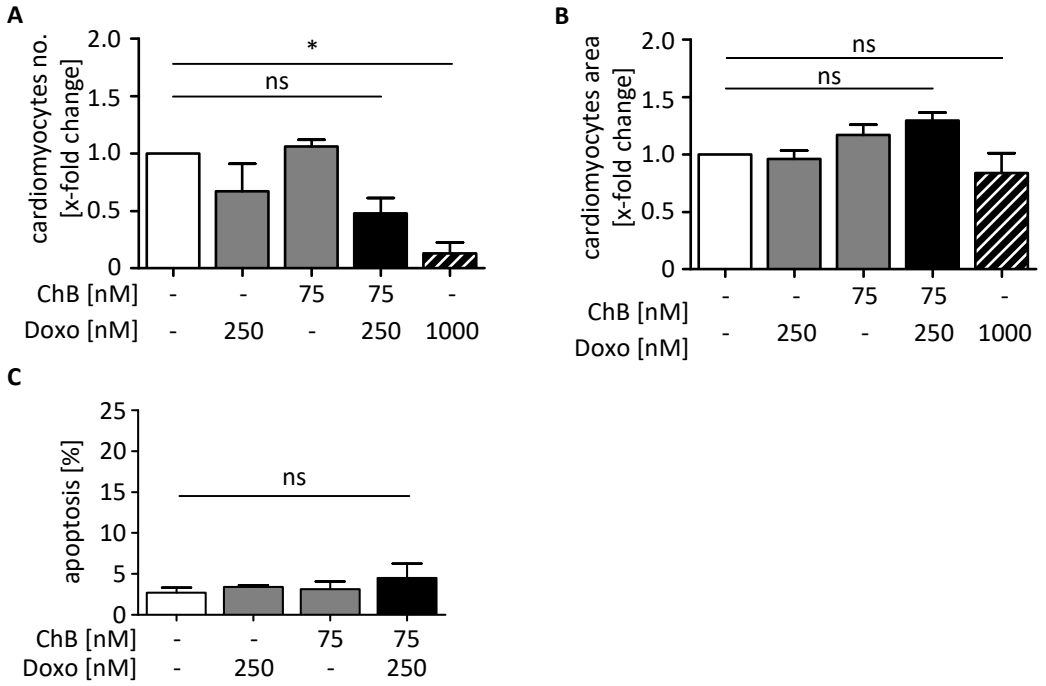

Figure 3.8: Clinical investigations with neonatal rat cardiomyocytes and human umbilical vein endothelial cells (HUVEC) after combination treatment. Non-cancer cells were treated with the indicated concentrations of chondramide B (ChB) and doxorubicin (Doxo). **A:** Neonatal rat cardiomyocytes number after 24 h treatment, 1000 nM Doxo indicates positive control. **B:** The quantification of cardiomyocytes area (α-actinin staining) after 24 h treatment represents an indicator for cardiac hypertrophy, n=3. **C:** Nicoletti assay of HUVECs after 48 h treatment, n=3. ns: not significant. One-Way-Anova/Bonferroni's Multiple Comparison Test, *$p < 0.05$. Experiments were conducted by Dr. Ramanujam (Pharmacology and Toxicology, TU Munich) and Alisa Krieg.

3.2 Inhibition of migration by actin binding compound miuraenamide A beyond actin hyperpolymerization

Besides the combination treatment of actin binding compounds with common chemotherapeutic drugs, another option is the clinical application of this compound class in single low dose treatment. Consequently, the structurally and functionally related miuraenamide (Miu) was analyzed in lower treatment concentration concerning the migratory inhibition of cancer cells.

3.2.1 Low dose Miu treatment slightly affected the cell functions

Miuraenamide A (Miu) is a potent actin hyperpolymerizing compound in higher concentrations and shows cytotoxic effects on various cancer cell lines.[37] A clinical low dose application of compounds is supposed to indicate lower side effects in patients. Therefore, an initial viability analysis of Miu treated SKOV3 cells was performed. The treatment with Miu led to a significant reduction of viability at concentrations of 25 nM or higher (Figure 3.9 A). Hence, the concentration of 20 nM, which showed no induction of apoptosis (Figure 3.9 B), was chosen for analyzing low dose effects of Miu on cancer cells. Notably, short term treatment with Miu displayed slight alterations of actin cytoskeleton after 2 h and 6 h. At this time points Miu led to actin agglomerates in the cytoplasm. In contrast, over longer periods of treatment from 24 h to 72 h the structure of actin cytoskeleton seems to be recovered, except after 56 h treatment (Figure 3.9 C). Here, the Miu treated cells showed slightly altered actin around the nucleus. Nevertheless, the actin cytoskeleton seems to be recovered over treatment for 72 h with Miu.

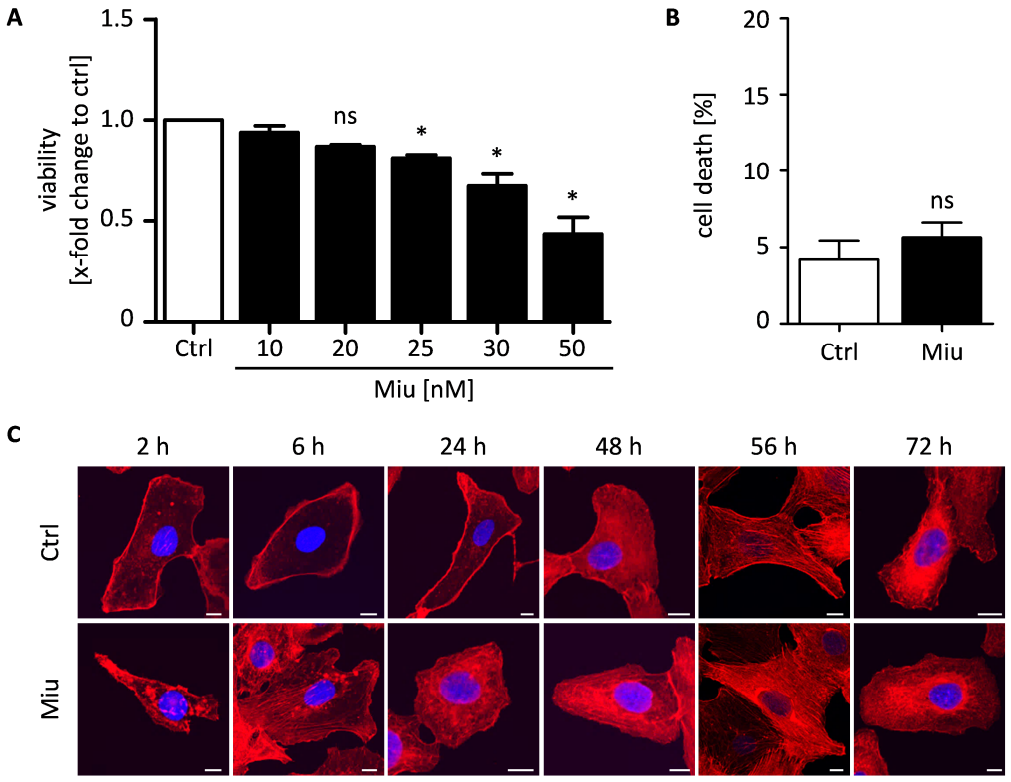

Figure 3.9: Low dose treatment of SKOV3 with miuraenamide A (Miu) showed slight effects on cell functions. A: Cell viability after treatment for 72 h of SKOV3 cells with the indicated concentrations of Miu, n=3. **B:** Cell death analysis after treatment for 72 h with 20 nM Miu, n=3. **C:** Immunostaining of SKOV3 cells treated with 20 nM Miu for the indicated time points. Stained for actin (rhodamine-phalloidin, red), and nucleus (Hoechst 33342, blue), n=3. White bars indicate 10 µm. ns, not significant. One-Way ANOVA/Bonferroni's Multiple Comparison Test, *$p < 0.05$.

3.2.2 Flow cytometry analysis indicated cell cycle alterations

Actin binding compounds are known to induce G_2/M phase arrest,[61] because of inhibition of cytokinesis, where the dynamic actin cytoskeleton is important.[62] Therefore, the cell cycle and cell size were analyzed. The FACS analysis showed a Miu induced G_2/M phase arrest after 72 h treatment in low dose treated SKOV3 cells, whereas, the size of cells remained unchanged. However, the inhibition of cell cycle seemed to be independent of alterations of the actin cytoskeleton and the results indicated alterations in cell homeostasis, even in low treatment concentrations with Miu.

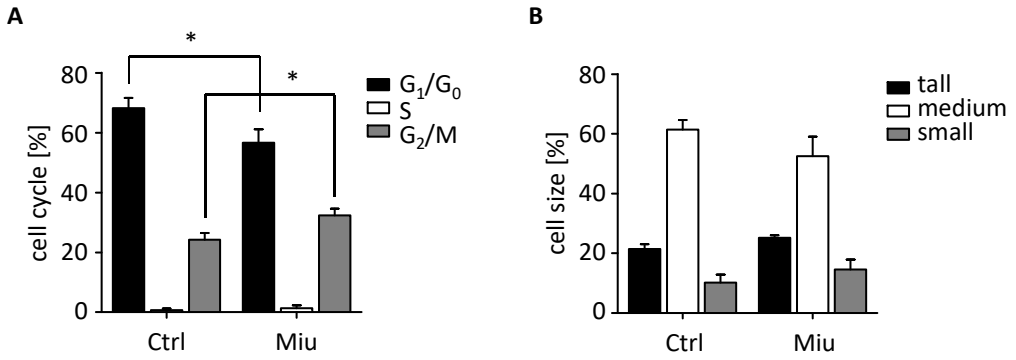

Figure 3.10: Cell cycle and cell size analysis of SKOV3 treated with miuraenamide A (Miu). SKOV3 cells were treated for 72 h with 20 nM Miu. **A:** Nicoletti cell cycle analysis, n=3. **B:** Flow cytometry analysis of cell size, n=3. Paired two tailed t-test, *p < 0.05.

3.2.3 Miu treatment specifically inhibited migration through pores

Previously, migration inhibitory effects could be achieved by treatment of cancer cells with the Miu related compound chondramide. Particularly, chondramide inhibited the migration of breast cancer cells, without inducing cell death.[34] Unlike the preceding experiments with chondramide, the following migration tests were performed after 72 h pre-stimulation with Miu, recovery of the actin cytoskeleton (72 h, Figure 3.9 C), and the absence of compound during assays (Figure 3.11). These treatment terms should exclude obvious actin disrupting effects of Miu and could elucidate an additional role of Miu treatment on cancer cells. First, the Boyden chamber migration assay was performed, where the cells have to push through restricted pores by deforming their cell shape and sensing the applied nutrition gradient (Figure 3.11 A). The pre-treatment with Miu indicated a reduction of migration to 0.58-fold of control cells (Ctrl). Moreover, migration

associated processes were analyzed. The first steps in the migration of cancer cells are the adhesion and spreading of cells on a surface.[63] These properties showed to be unaffected by Miu treatment (Figure 3.11 B). Further, the exact mechanism and reason for inhibited cell migration through pores were elucidated. To this end, the wound healing assay was performed. The Miu treated SKOV3 cells showed similar wound closure, comparable with untreated cells, whereas the negative control cells (neg Ctrl), which were cultivated in FCS free medium, indicated almost no migration (Figure 3.11 C). Furthermore, the secretion property of Miu treated HeLa_ssHRP cells was investigated. Those cells are stable transfected with a horse radish peroxidase (HRP) construct, which is tagged to a signal sequence (ss) for secretion.[64] The secretion of migration stimulating factors is known to be important for the sufficient migration.[65] Therefore, the stable transfected HeLa cells were used for analyzing cell transport machinery via the quantification of extracellular secreted HRP. The positive control treatment with brefeldin A impaired the HRP secretion during four hours, by preventing vesicle transport from the endoplasmic reticulum to the Golgi complex. Conversely, this was not the case for the Miu 20 nM pre-treatment or the repeated Miu stimulation over four hour secretion (Figure 3.11 D). To elucidate the effect of Miu treatment on the sensing of nutrition, the chemotaxis migration assay was conducted (Figure 3.11 E). The forward migration index (FMI) of SKOV3 cells and the velocity were not influenced by Miu and showed no significant inhibition after Miu treatment. From this data, we could conclude an inhibitory effect on SKOV3 cell migration after Miu pre-treatment, which could be shown in restricted migration and seemed to be deformation dependent. The examination of other migration assays like the wound healing, HRP secretion, and chemotaxis assay, demonstrated unaltered migration behaviors after Miu treatment.

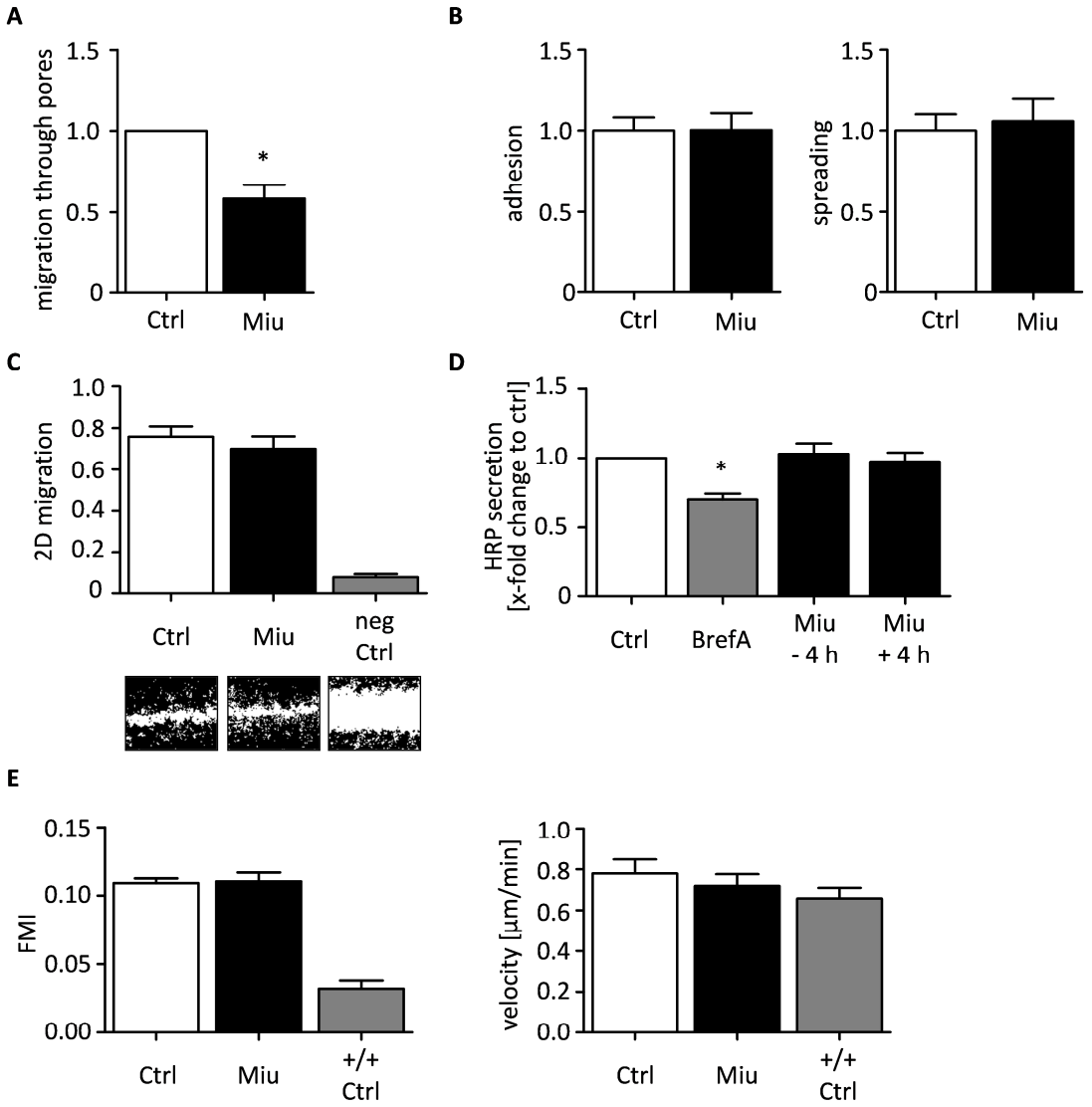

Figure 3.11: Analysis of migration and associated parameters. SKOV3 cells were pre-treated with 20 nM Miu over 72 h, during migration analysis no compound was present. **A:** Boyden chamber migration assay over 24 h migration through 8 µm pore membrane, n=4. **B:** Migration associated parameters, adhesion and spreading, quantified by counting adhered or spread cells, n=3-4. **C:** Wound healing assay, neg Ctrl: negative control, migration in FCS free medium. One representative image per treatment is shown, n=4. **D:** HRP secretion assay with HeLa_ssHRP, brefeldin A (BrefA) was used as positive control, fresh Miu was added (+4 h) or not (-4 h) during secretion, n=4. One-Way ANOVA/Bonferroni's Multiple Comparison Test, *p < 0.05. **E:** Chemotaxis migration assay over 24 h migration along an FCS gradient. FMI, forward migration index, +/+ Ctrl: positive control, medium with FCS without FCS gradient, n=3. Paired two tailed t-test, *p < 0.05.

3.2.4 Stiffness of the cell nucleus was altered by Miu treatment

The degree of cancer cell rigidity has previously been shown to be lower in comparison to non-cancer cells.[66] Furthermore, the nucleus is the largest organelle in the cell and is supposed to be the limiting factor during migration through restricted pores.[53,67] Therefore, the mechanical properties of cells were elucidated by stiffness measurements. SKOV3 cells were treated with Miu for 72 h and the stiffness was measured with the atomic force microscope. The total cell stiffness was recorded by a defined force map of 80x80 µm. The stiffness of nucleus could be determined by applying a specific force on the cell nucleus and both were calculated with the young's moduli (see 2.9.3). The total cell stiffness of Miu treated SKOV3 cells was unaffected after treatment for 72 h (Figure 3.12 A), whereas the stiffness of the nuclei showed alterations (Figure 3.12 B). The Miu treated cells displayed an enhancement of nuclear stiffness of 1.4-fold compared to control cells. These data indicated the influence of Miu low dose treatment on the mechanical properties of the cancer cell nuclei.

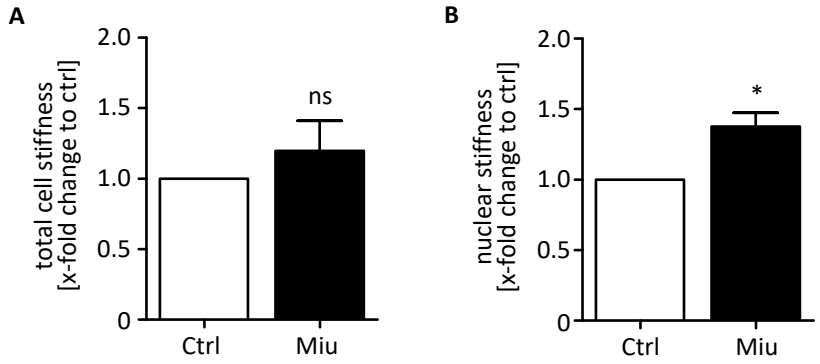

Figure 3.12: Atomic force measurements of Miu treated SKOV3 cells. Cells were treated for 72 h with 20 nM miuraenamide (Miu) or DMSO as solvent control (Ctrl). **A:** Total cell stiffness was measured with a force map of 80x80 µm in contact mode, nine maps per experiment were measured, n=4, normalized young's modulus/kPa **B:** Nuclear stiffness measurement with single force curves in contact mode, 10-20 cells per experiment were measured, n=4, normalized young's modulus/kPa. Paired two tailed t-test, *$p < 0.05$. ns: not significant. The measurements were performed by Daniel Ruediger.

3.2.5 Miu treatment had an impact on three dimensional migration

According to the stiffness measurements and Boyden chamber migration assays, life cell imaging was performed to visualize the three dimensional (3D) migration of SKOV3 cells after 72 h Miu stimulation. The migrating cells have to push through the confined network in the 3D environment and should be able to deform, while moving on their track. The pre-treated cells were seeded into rat tail collagen I gels with a concentration of 2 mg/ml and imaged over 20 h. The cellular phenotypes were separated into four groups: sprouting, squeezing, immobile, and dying (Figure 3.13). The sprouting type indicates cells, which create cellular protrusions, whereas the squeezing cells are ones, which manage the track limitation by pushing through restricted pores in the network. Further, immobile cells showed no protrusions and the dying cells depicted apoptotic bodies and cell fragmentation. The SKOV3 cells, which were treated with Miu, showed slightly fewer cells with sprouting and more immobile cellular phenotypes by trend. Moreover, Miu treatment indicated a lower amount of cells, which squeezed through restrictions on their migration track, whereas, cell death was just slightly increased in 3D migration of Miu treated SKOV3 cells. This data supports the Boyden chamber migration assay and the results of nuclear stiffness measurement. In conclusion, the 3D migration through a restricted network is inhibited by Miu treatment.

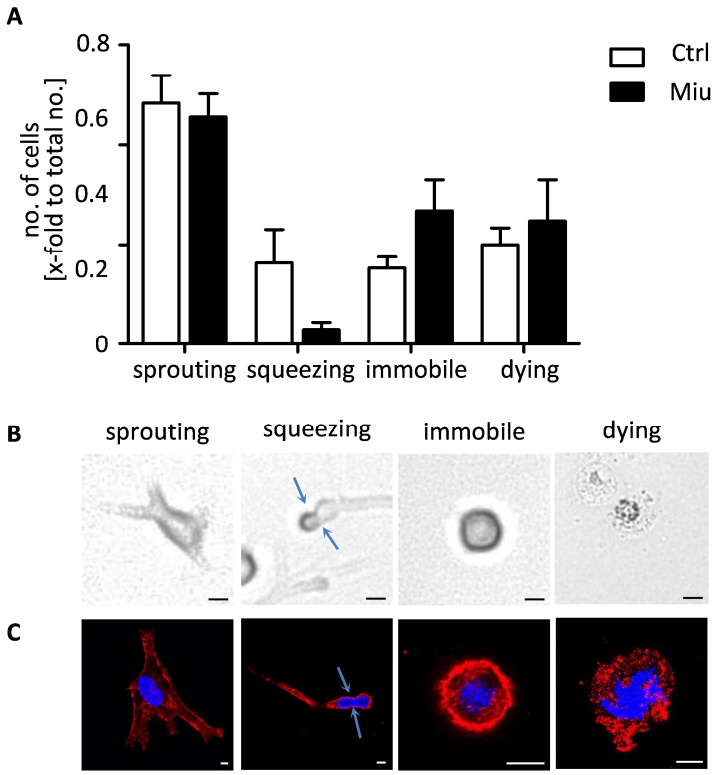

Figure 3.13: Rat tail collagen I 3D gel migration of SKOV3 cells. Cells were pre-treated for 72 h with 20 nM miuraenamide (Miu) and migrated over 20 h in collagen I gels (2 mg/ml). **A:** Quantification of cellular phenotypes normalized to total counted cell number (total no.), n=3. **B:** Example images of cellular phenotypes recorded by life cell imaging with transmitted light microscopy, n=3. **C:** Example images of cellular phenotypes depicted with fluorescence microscope, stained for actin (rhodamine-phalloidin, red), and nucleus (Hoechst 33342, blue), n=3. Black and white bars indicate 10 µm. Blue arrows depict the deformed nucleus due to restriction.

3.2.6 Proteome analysis indicated regulated proteins after treatment for 56 h

We were interested in the amount of proteins affected by Miu treatment to elucidate the responsible signaling mechanisms for changes of nuclear stiffness. Therefore, the proteome analysis of Miu treated SKOV3 cells was performed over a treatment period of 96 h. The alterations of 7328 proteins were recorded after Miu treatment over time with the MaxQuant proteome analysis. The heat plot depicted clusters with up- or down-regulated proteins at earlier time-points (red or green, Figure 3.14 A), which could be explained by counter regulatory mechanisms or the alteration of actin regulated transcription factors due to actin agglomerations after approximately 4 h stimulation.[20] Furthermore, two prominent clusters were found after treatment for 56 h, which were analyzed further (Figure 3.14 B). A few actin associated proteins were up-regulated at this

time point (B, red graph), whereas the enrichment analysis of down-regulated proteins after treatment for 56 h showed different regulated pathways (Figure 3.14 C). The pathways with a false discovery rate (FDR)[60] of < 0.2 (orange dots) and enrichment values of > 2 (red dots) were determined as important altered pathways (Wnt-signaling pathway, autophagy, Epithelial cell signaling in *H. pylori* infections), whereas KEGG Wnt-signaling pathway indicated 17 proteins with an enrichment of 3.33 and FDR of 1.37×10^{-3}. The 17 proteins of Wnt-signaling pathway in the down-regulated 56 h treatment cluster are listed in Table 3.1 and depicted a highly connected network (Figure 3.14 D). This indicated the highest influence of Miu treatment on Wnt-signaling pathway. In conclusion, the proteome analysis showed alterations of the Wnt-signaling pathway after Miu treatment eight hours before 3D migration was inhibited (Figure 3.11). The marked Wnt-signaling proteins in Table 3.1 were supposed to be regulated by actin and indicated transcription regulating activity. For instance, the function of nuclear factors of activated T-cell (NFATs) was associated to actin cytoskeleton and actin regulates the nuclear duration of this transcription factor.[68,69] Likewise, the histone acetyltransferase p300 turned out to be down-regulated in proteomics and implicated the link to actin cytoskeleton via the transcription co-activator MRTF-A.[70] For these reasons, the Wnt-signaling and the mentioned actin associated proteins were further analyzed.

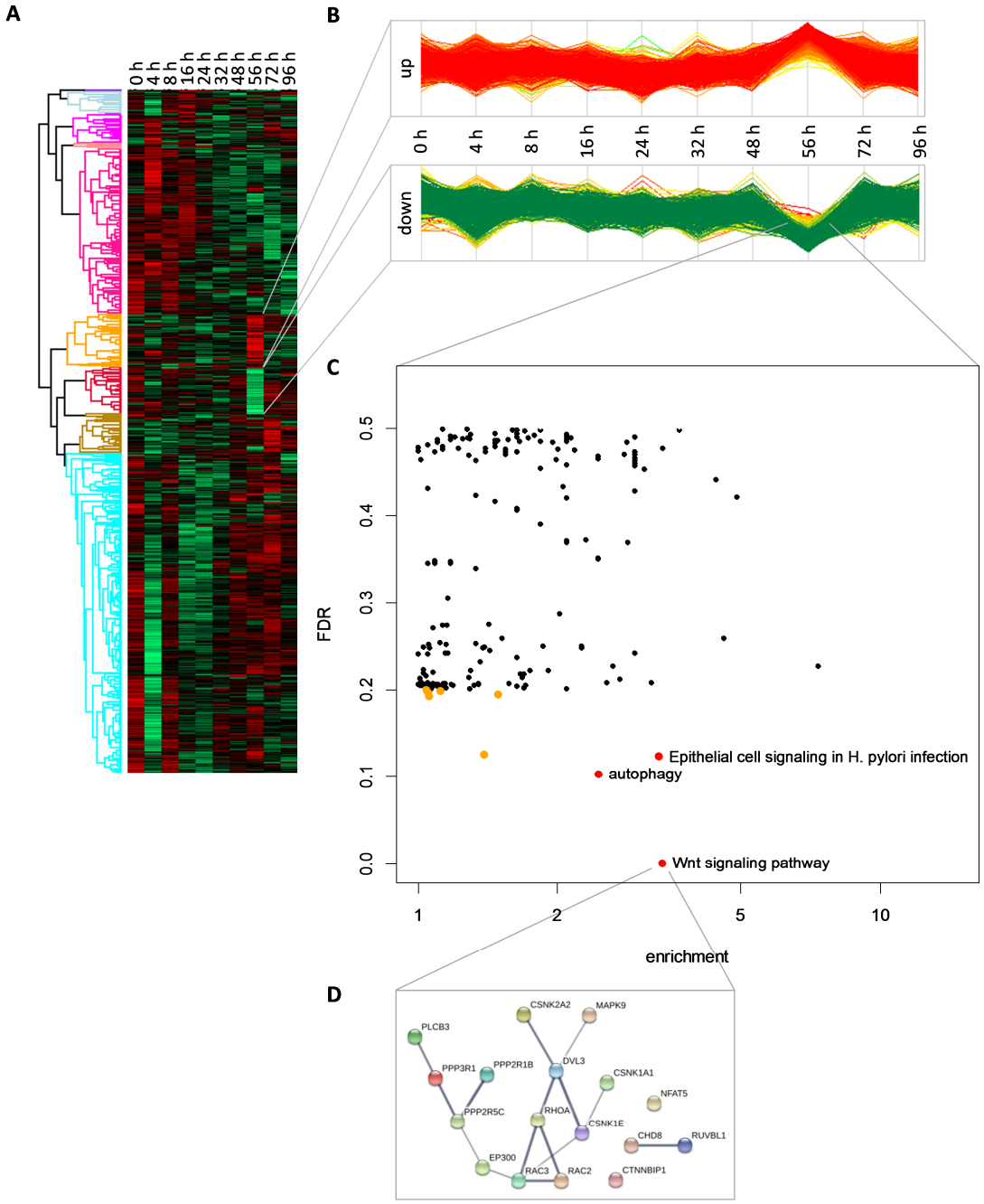

Figure 3.14: Proteome analysis with MaxQuant, Perseus data processing and StringDB analysis. SKOV3 cells were treated with Miu 20 nM for indicated time points. **A:** Heat plot with ten defined row clusters, red areas indicate up- and green areas indicate down-regulation. **B:** Defined cluster up- and down-regulated proteins after 56 h treatment depicted in lanes as time series. **C:** Dot plot of enriched pathways with a threshold of FDR < 0.5 showed down-regulated proteins after 56 h treatment, orange dots: FDR < 0.2, red dots: FDR < 0.2 and enrichment value > 2. **D:** StringDB analysis of highest pathway enrichment (Wnt-signaling) in indicated cluster. Interaction sources were adjusted to experiments, databases, co-expression, neighborhood, gene fusion, and co-occurrence. Minimum required interaction score was 0.4, whereas thicker and darker gray connections represent higher confidence of interaction score. Proteome analysis with MaxQuant and Perseus data processing was conducted by Dr. Yu (Proteomics and Bioanalytics TU Munich).

Table 3.1: Genes of Wnt-signaling enrichment

No	Gene names	Protein names
1	CHD8	Chromodomain-helicase-DNA-binding protein 8
2	CSNK1A1	Casein kinase I isoform alpha
3	CSNK1E	Casein kinase I isoform epsilon
4	CSNK2A2	Casein kinase II subunit alpha
5	CTNNBIP1	Beta-catenin-interacting protein 1
6	DVL3	Segment polarity protein dishevelled homolog DVL-3
7	**EP300**	**Histone acetyltransferase p300**
8	MAPK9	Mitogen-activated protein kinase 9
9	**NFAT5**	**Nuclear factor of activated T-cells 5**
10	PLCB3	1-phosphatidylinositol 4,5-bisphosphate phosphodiesterase beta-3
11	PPP2R1B	Serine/threonine-protein phosphatase 2A 65 kDa regulatory subunit A beta isoform
12	PPP2R5C	Serine/threonine-protein phosphatase 2A 56 kDa regulatory subunit gamma isoform
13	PPP3R1	Calcineurin subunit B type 1
14	RAC2	Ras-related C3 botulinum toxin substrate 2
15	RAC3	Ras-related C3 botulinum toxin substrate 3
16	RHOA	Transforming protein RhoA
17	RUVBL1	RuvB-like 1

3.2.7 Miu treatment impaired Wnt-signaling transcription factors

The transcription factor β-catenin is one of the key activators of Wnt-signaling, and it is mobilized by uncoupling from inhibitors and translocation to the nucleus.[71] The ability of β-catenin to bind to the TCF/Lef1 promoter and to activate the transcription could be tested by the luciferase reporter gene assay. The promoter plasmid pFOPFlash (mutant pTOPFlash) was transfected to exclude the unspecific effects of Miu treatment on transcription. Notably, the activation of promoter and transcription of luciferase was not affected by Miu treatment (Figure 3.15). Nevertheless, it should be noticed that TCF/Lef1 could also be activated independent from β-catenin.[72]

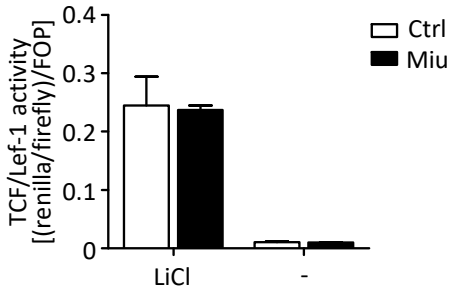

Figure 3.15: β-catenin promoter TCF/Lef1 reporter gene assay. Cells were treated for 56 h with 20 nM miuraenamide (Miu) and/or LiCl 40 mM. The signal of renilla luciferase activity was normalized to firefly (constitutive active promoter) and pFOPFlash (TOPFlash mutant), n=3.

Subsequently, the translocation and hence the activation of β-catenin and NFAT5 to the nucleus was analyzed. First, β-catenin localization after stimulation with LiCl and simultaneous treatment with Miu was examined. The quantification showed a translocation of β-catenin to the nucleus after LiCl stimulation, which indicated a trend to inhibition after Miu treatment for 56 h (Figure 3.16 A). Additionally, the non-canonical, β-catenin independent transcription factor NFAT5[73] was stained for nuclear localization after Miu treatment (Figure 3.16 B). The translocation of NFAT5 was also inhibited by trend after Miu treatment and indicated a more general inhibition of transcription factor translocation by Miu treatment.

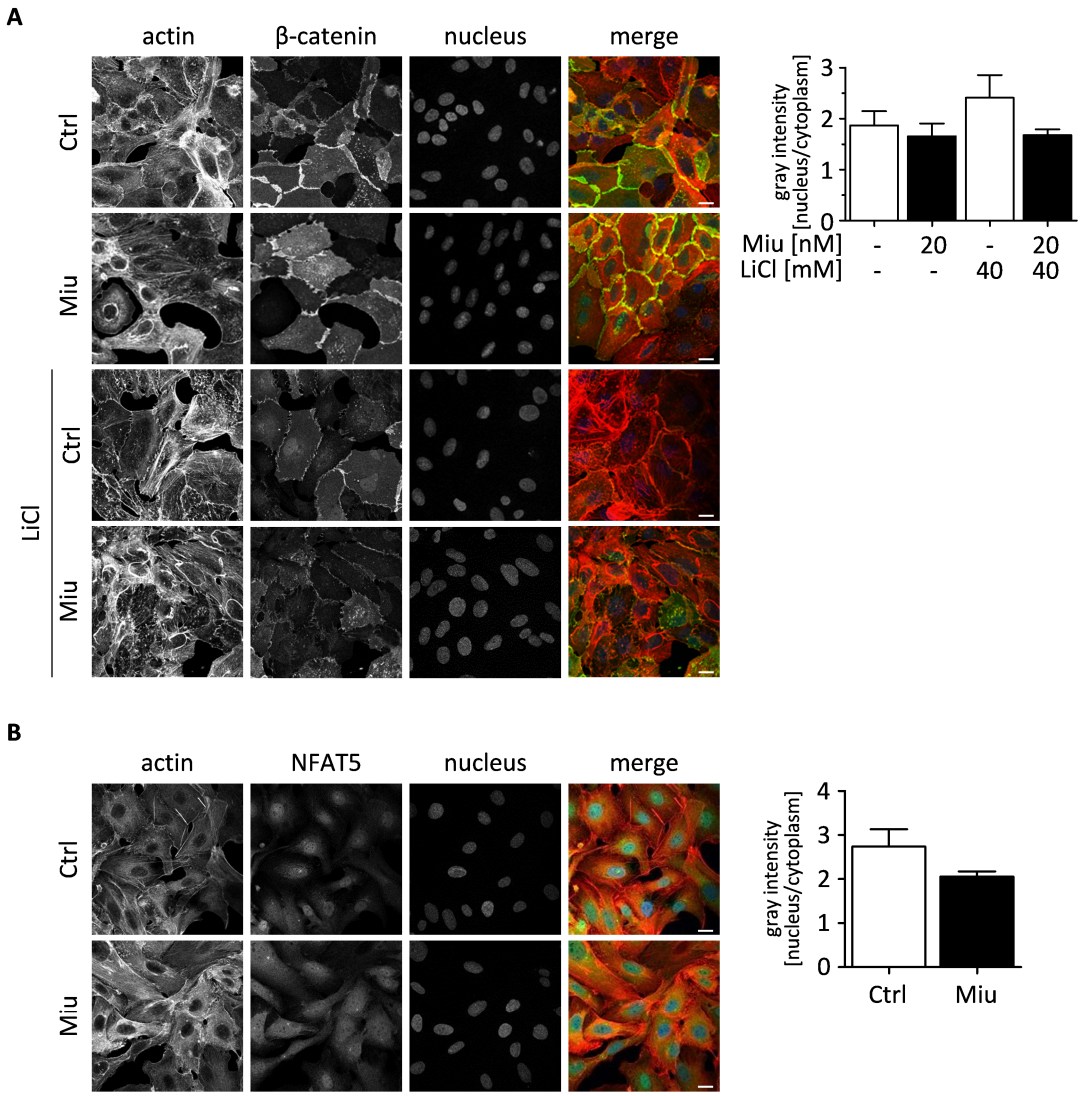

Figure 3.16: Confirmation of Wnt-signaling pathway alteration. SKOV3 cells treated with 20 nM Miu for 56 h. **A:** Immunostaining of β-catenin after Miu and/or LiCl 40 mM stimulation, and the quantification of nuclear localization (bar diagram), β-catenin (antibody, green), n=3. **B:** Immunostaining of NFAT5 after Miu stimulation, and the quantification of nuclear localization (bar diagram), NFAT5 (antibody, green), n=3. One representative image per treatment is shown. Staining of actin (rhodamine-phalloidin, red) and nucleus (Hoechst 33342, blue). White bars indicate 20 µm.

3.2.8 Miu treatment reduced the protein level of p300

The histone acetyltransferase p300 (also EP300) is a transcription co-activator, which is crucial for the expression of many proteins and is overexpressed in different cancers.[74] It is important in Wnt-signaling and builds multi-protein complexes with transcription factors like β-catenin[75] or MRTF.[70] Figure 3.17 A depicts the immunostaining of the transcription co-activator p300 and indicated that the nuclear localization of p300 was not impaired by Miu treatment. Furthermore, the protein level of p300 was analyzed after stimulation for 56 h with Miu. The treatment showed a down-regulation of protein levels to 0.6-fold compared to control (Figure 3.17 A). The mRNA level was also affected by Miu treatment (0.8-fold), which indicated a reduction of p300 expression. This reduction of protein level seemed to be reduced at least in part by impaired p300 mRNA transcription (Figure 3.17 B). These data emphasized the influence of Miu treatment on the p300 transcription co-activator expression and confirmed the evidence of proteome examination after Miu treatment for 56 h.

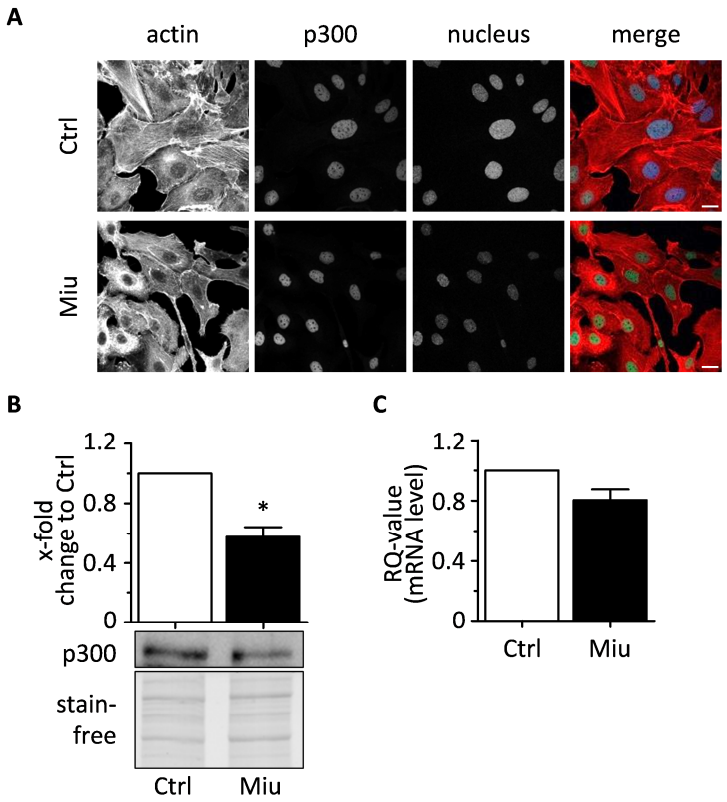

Figure 3.17: Localization and expression analysis of p300 on protein and mRNA level. SKOV3 cells were treated with 20 nM Miu for 56 h. **A:** Immunostaining of p300 (antibody, green), actin (rhodamine-phalloidin, red) and nucleus (Hoechst 33342, blue), n=2. White bars indicate 20 µm. **B:** Protein level of p300 with the quantification. One representative image per treatment is shown, n=4. **C:** RQ-values of p300 mRNA level, n=2. Paired two tailed t-test, *p < 0.05.

3.2.9 MRTF-related genes were down-regulated by Miu treatment

The proteome data was analyzed concerning MRTF-regulated or associated genes. The selection of genes was collected by GeneCards®[76] Keyword Search "MRTF" (Table 3.2). Notably, most of the listed genes are down-regulated by Miu treatment (Figure 3.18). A few of them strongly related to migration regulating processes. For instance, LIMA1 expression (also called Eplin) is regulated by MRTF,[77] and showed lower protein levels after Miu treatment in proteome analysis. Proteins, which are known for their interaction with MRTF and simultaneously regulate migration processes, like SMYD3[78] and MICAL[79], were expressed in lower levels in comparison to control. Likewise, importins, which regulate nuclear MRTF transport (KPNA3, KPNB1)[80], were down-regulated after Miu treatment. Hence, the data strongly indicated the alteration of MRTF-related genes in a migration regulating context after Miu low dose treatment.

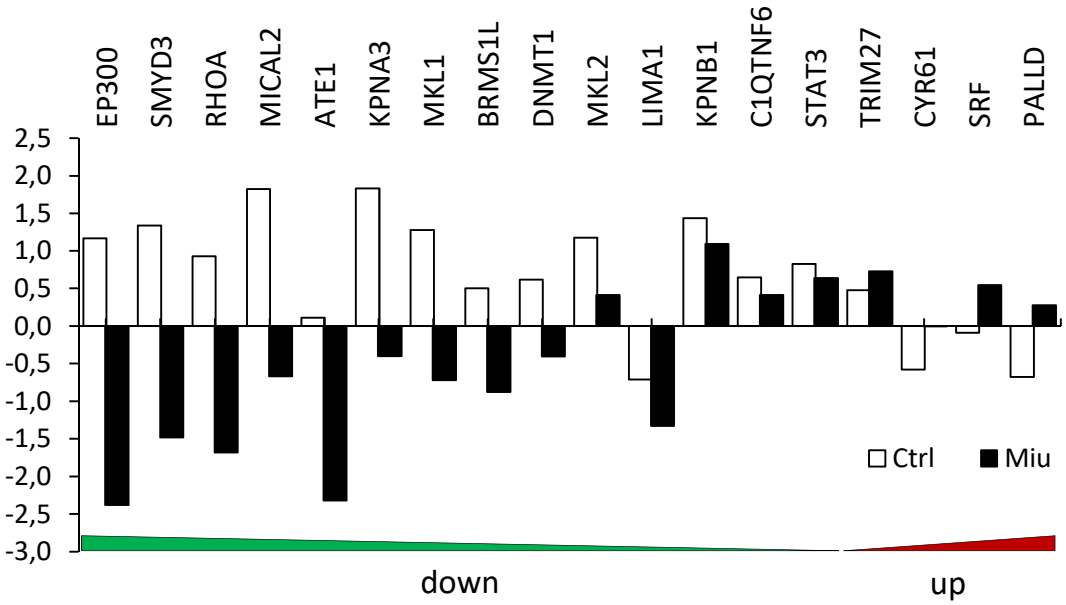

Figure 3.18: Proteome analysis of MRTF-associated genes. SKOV3 cells were treated with 20 nM miuraenamide for 56 h (Miu, black bars) or harvested at stimulation start point without treatment (Ctrl, white bars).

Table 3.2: Proteome analysis of MRTF-associated genes

No	Gene name	Protein description
1	ATE1	Arginyl-tRNA-protein transferase 1
2	BRMS1L	Breast cancer metastasis-suppressor 1-like protein
3	C1QTNF6	Complement C1q tumor necrosis factor-related protein 6

No	Gene name	Protein description
4	CYR61	Protein CYR61
5	DNMT1	DNA (cytosine-5)-methyltransferase 1
6	EP300	Histone acetyltransferase p300
7	KPNA3	Importin subunit alpha-4
8	KPNB1	Importin subunit beta-1
9	LIMA1	LIM domain and actin-binding protein 1, also Eplin
10	MICAL2	Protein-methionine sulfoxide oxidase MICAL2
11	MKL1	MKL/myocardin-like protein 1
12	MKL2	MKL/myocardin-like protein 2; Phosphatase and actin regulator
13	PALLD	Palladin
14	RHOA	Transforming protein RhoA
15	SMYD3	Histone-lysine N-methyltransferase SMYD3
15	SRF	Serum response factor
17	STAT3	Signal transducer and activator of transcription 3; Signal transducer and activator of transcription
18	TRIM27	Zinc finger protein RFP

The transcriptional co-activator p300 interacts with the transcription factor MRTF-A and the interaction proved to activate migration regulatory genes.[70] Therefore, the gene expression of CYR61, which is a migration-related gene regulated by MRTF-A, was examined (Figure 3.19). The treatment of SKOV3 cells over 72 h with Miu showed a significantly reduced expression level of CYR61 (0.8-fold). After treatment for 56 h, no alteration of the CYR61 mRNA level was detectable, indicating a time-dependent regulation of CYR61, which is down-stream of p300 expression reduction.

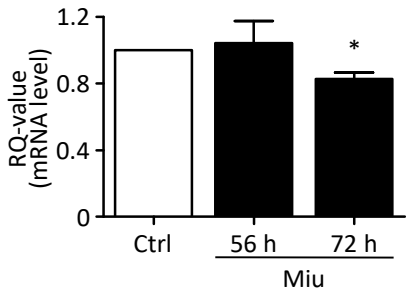

Figure 3.19: Expression analysis of CYR61 mRNA level. SKOV3 cells were treated with 20 nM Miu for 56 h or 72 h. RQ-values of CYR61 mRNA level, n=3. Paired two tailed t-test, *p < 0.05.

4 DISCUSSION

4.1 Cytoskeletal binding compounds in clinical use

Natural compounds, which influence the cellular cytoskeleton, have been used very successfully for decades in cancer treatment. Microtubule manipulating substances such as paclitaxel, epothilone or colchicine, are not only established in the clinic for cancer treatment, but also amongst others, for the treatment of inflammatory disease.[31,81] However, a pharmacological therapy of patients suffering from cancer with actin binding compounds is still missing, although numerous studies have pointed out the effectiveness against tumor cells *in vitro* and *in vivo*.[33,34,37] The incidence of side effects and resistant mechanisms are still the limiting factors for the approval of actin binding compounds and chemotherapeutic drugs in general. Known resistance mechanisms are, e.g., the induction of efflux pump expression in line with the multidrug resistance (MDR) gene activation, mutations of target enzymes, enhanced drug degradation, or increased DNA damage repair.[82] Limitations are also given by life-threatening side effects as cardiotoxicity, nephrotoxicity or neurotoxicity.[49]

Modern clinical approaches concentrate on circumventing those resistance mechanisms and attempt to decrease side effects. For instance, side effects could be reduced by chemotherapy consisting of the combination of treatments with two or more compounds. But most of the applied combinations are empirically designed and concentrate on pharmacokinetic profiles or biological interactions between drugs.[83] Thus, the understanding of mechanisms, which lead to synergistic effects of distinct drug combinations, could further improve cancer therapy. Novel chemotherapeutic drugs might target counter regulatory mechanisms of one combination partner and therefore achieve greater therapeutic success. Herein, we represented two novel approaches in order to decrease limiting side effects of cancer therapy and to elucidate underlying mechanisms.

4.2 Combination treatment with doxorubicin and chondramide B

This study pointed out that the successful combination of actin binding compound ChB and DNA damage induction emerged from increased DNA damage due to altered DNA damage response (DDR). We elucidated the synergistic mechanism and demonstrated the implication of the Golgi complex in this process.

Mechanisms of DNA damage response are known to be linked to organelle function in the cell. For instance, the tumor suppressor protein p53 links DDR to mitochondria in order to induce mitochondrial release of cytochrome C, leading to the induction of intrinsic apoptosis.[84] Whereas the mitochondria and the nucleus represent well-known organelles in DDR, the role of the Golgi complex is poorly understood. Only recently, the Golgi complex has been described to be crucial in DDR.[43]

The first part of this study followed a novel approach, where the Golgi dependent DDR could be prevented. In particular, the Golgi complex localization was altered by inhibiting actin dynamics after chondramide (ChB) treatment. Farber-Katz described a DDR signaling cascade, based on the Golgi phosphoprotein 3 (GOLPH3), which most probably regulates the transport processes between the nucleus and the plasma membrane. They postulated the activation of the GOLPH3 dependent signaling cascade after DNA damage induction. The DNA dependent protein kinase (DNA-PK) is activated and led to a force transmission from GOLPH3 to myosin 18A (Myo18A) by means of the actin cytoskeleton. The group indicated the importance of the Golgi complex dependent signaling cascade for the survival of cancer cells.[43] In addition, we could show that cancer cells reacted sensitive to the inhibition of Golgi dispersal by chondramide treatment, which led to a hyperpolymerization of actin. Comparable effects were observed by DNA damage induction and simultaneous inhibition of DNA-PK, which triggers the DDR and activates the signaling cascade, ending in disrupted Golgi dynamics.

4.2.1 Inhibition of GOLPH3 pathway is a potential target in cancer therapy

According to the outlined implication of Golgi dispersal in DDR, proteins of the GOLPH3 signaling cascade can serve as a target for cancer therapy. Notably, the Golgi complex-associated GOLPH3 is overexpressed in many cancer types and is known to correlate with a poor prognosis in several cancerous diseases.[85-87] It is located at the *trans*-Golgi

membrane via a phosphatidylinositol-4-phosphate (PI4P) link and is known to be important for Golgi trafficking.[88,89] The primary function of the Golgi complex is the processing of glycosylated proteins and is therefore important for the activation of various proteins and receptors.[90,91]

In particular, members of the toll like receptor (TLR) family are activated by glycosylation, which further leads to a proper localization and function of the receptors.[92] Interestingly, the TLR activation was described to increase DNA damage repair.[93] Moreover, DNA repair enzymes, like ATM[94] and DNA-PK[95], are supposed to be activated or persist longer in an activated state due to glycosylation. The relation of GOLPH3 pathway inhibition, followed by a reduction of the nucleus to plasma membrane transport, might links the Golgi dispersal to DNA damage repair mechanisms.

Secretion processes do not exclusively rely on GOLPH3, but also on its interaction partner Myo18A.[89] The unconventional Myo18A contains an actin binding domain, by which it interacts with actin filaments and transmits the signal for Golgi dispersal to the actin cytoskeleton. Consequently, Myo18A links the actin cytoskeleton to the DDR. We could show that treatment with ChB results in entrapment of Myo18A in actin agglomerates and therefore leads to an impairment of its localization. Likewise, previous studies with ChB demonstrated the trapping of other oncoproteins in actin agglomerates followed by specific cancer cell death induction.[33]

Our group demonstrated the feasibility of actin binding drugs, like ChB, for the use in cancer therapy, by targeting known cancer signaling pathways. We provided a new combination approach for inhibiting GOLPH3 signaling transduction via the trapping of Myo18A, which further leads to the disruption of Golgi complex dependent DDR. Although, targeting GOLPH3 in cancer cells seems to be an appropriate approach for fighting cancer, to our knowledge, no inhibitor exists. With the combination of Doxo, DNA damage induction and inhibition of Golgi complex dependent DDR via ChB treatment, we provide a novel combination therapy based on the knowledge of counter regulatory mechanisms.

4.2.2 Cell line specific effects confirm the importance of Golgi dispersal

The implication of the Golgi complex in DDR has been poorly studied, but represents a promising target in cancer therapy. In order to gain further insight, we examined different cell types to define the specificity of treatment in various cell lines. Notably, the combination treatment of Doxo and ChB elucidated a cell line specific cell death response, which could be attributed to an altered Golgi complex dependent DDR. SKBR3 cells, in contrast to MDA-MB-231 and T24 cells, displayed no Golgi dispersal after DNA damage induction with Doxo. After the simultaneous treatment with Doxo and ChB the localization of the SKBR3 Golgi complex remains stable in comparison to the responding cell lines. Accordingly, the combination treatment did not have an impact on cell death induction of SKBR3 cells. The specific response of cell lines after DNA damage on the function of organelles was described before. Whaba *et al.* tested the translatome in three glioblastoma cancer cell lines after ionizing radiation and showed cell-line specific changes in mitochondria.[96] Obviously, the response of cell organelles seemed to vary among cancer cell lines. The importance of the Golgi dispersal for DNA damage repair was emphasized, by the results of SKBR3 cells, which showed no induction of DNA damage and cell death after combination treatment. The success of combination treatment has previously turned out to be limited. For instance, the combination of tamoxifen, which targets estrogen receptor (ER)-positive breast cancer, with classic cytostatic drugs showed positive results in clinical trials, but may have no impact on ER-negative breast cancer tissue.[97] Thus, the impact of precision medicine increases continuously and pre-clinical tests like microarray analysis of tumor markers have been implicated in cancer therapy.[98] On the one hand the cell line specificity of Doxo and ChB combination treatment reflects the limitations of combination treatment, but on the other hand it could establish the Golgi dispersal as a novel predictor of therapy effectiveness in cancer treatment.

4.2.3 Benefits and risks of targeting the actin cytoskeleton

Equally important to the knowledge of cancer signaling targets are the presence or absence of side effects. Prior to the application in the clinic, drugs have to be proved on efficacy and safety. The occurrence of side effects represents one important limiting factor in clinical trials. Thus, secondary effects in patients could be diminished by reducing

the treatment dose and by applying more than one compound. The combination therapy should exclude negative interactions or additive side effects, like cardiotoxicity. For instance, Doxo inhibits cancer cell growth and induces DNA damage by diverse modes of actions, but induces prominent side effects in patients. Besides the inhibition of topoisomerase II, Doxo affects the mitochondrial electron transport chain, which was supposed to be responsible for the considerable cardiotoxicity of Doxo therapy.[49] Interestingly, the treatment with actin hyperpolymerizing compound jasplakinolide also showed toxic effects on cardiomyocytes due to inhibition of cardiac ion channel activity.[99] Furthermore, the treatment with actin disrupting agent cytochalasin D displayed dysfunctional volume regulations of neonatal rat cardiomyocytes.[100] We observed the effect of the combination treatment of ChB and Doxo on cardiomyocytes and endothelial cells. In contrast to the results with the previously stated actin binding compounds, this study demonstrates the actin binding compound ChB as an appropriate combination partner for Doxo. The single treatment with ChB did not have an impact on cardiomyocytes. Additionally, in combination with Doxo, ChB did not show an undesirable effect on cardiomyocytes number and area. Thus, the combination of ChB and Doxo displayed a substantial lower effect on cardiomyocyte compared with Doxo single standard dose treatment of 1000 nM.[101]

We also investigated the effects on human umbilical vein endothelial cells (HUVECs) as a model for physiological blood vessel endothelium.[102] Higher treatment concentrations of Doxo are known to induce DNA damage and cell death in HUVECs.[103] Notably, we showed, that the apoptosis rate of HUVECs was unaffected by lower Doxo concentration in single or combination treatment. Accordingly, the observed body weight of mice indicated a good tolerance of combined therapy *in vivo*. These findings reinforce the potential of actin binding compounds for Doxo treatment combinations to reduce limiting side effects.

4.3 Low dose miuraenamide beyond actin hyperpolymerization

Various studies discussed the migration inhibitory effect of actin binding compounds and demonstrated the importance of the actin cytoskeleton for the mobility of tumor cells.[34,104] However, those effects could be explained by primary effects on the actin structure. Miuraenamide, similar to ChB, stabilizes the filament form of actin and has inhibiting effects in cancer growth with concentrations of IC_{50} values from 3.7 nM to 79.6 nM.[37] Also in migration inhibitory experiments, prominent actin alterations were visible in rhodamine-phalloidin staining, where the actin structure is disrupted to actin agglomerates. Those effects were prominently detected after treatment with high concentrations of the actin binding compound. The cancer cells were usually treated for a short period of time and compounds were present during the migration assays. Previous results of our group indicated inhibitory effects of ChB treatment on migrating cancer cells due to an alteration of stress fiber formation and inhibition of RhoA signaling. The strong effect on the actin cytoskeleton after 8 h treatment was improved after the removal of ChB. Recently research investigated the same recovery of actin cytoskeleton after compound removal. Lazaro-Dieguez *et al.* provided evidence for the participation of autophagosomal degradation of the actin agglomerates.[105] On the contrary, the cancer cells in this study were incubated over a few days with low doses of Miu without removing the compound. With the lower dose treatment, the cytoskeletal actin structure recovers in the presence of Miu. Hence, we showed migration inhibitory effects of Miu beyond the disruption of the actin cytoskeleton.

4.3.1 Effects of Miu low dose treatment on the migration through pores

We could show specific inhibitory effects of Miu after visible recovery of the actin cytoskeleton. The treatment with a concentration of 20 nM showed no effect on viability and cell death induction after 72 h, which represents the starting point of investigations. Furthermore, the first hint of an altered cellular state after long term treatment with Miu was a slight increase of G_2/M phase arrest. The alteration of cell cycle due to actin binding compounds was described previously, but as stated earlier, in these cells the effect could be attributed to huge alterations of the actin cytoskeleton due to the higher treatment concentrations.[61]

The key experiment represented the impaired migration of ovarian cancer cell line SKOV3 during Boyden chamber migration assay. Notably, we showed the inhibition of migration after 72 h treatment with low dose Miu concentration, which was not dependent on alteration of adhesion or spreading processes of cancer cells. To clarify the exact mechanism, further migration assays were conducted. Interestingly, the mobility of SKOV3 cells was not inhibited in wound healing assay. In addition, we wanted to elucidate the consequences of Miu treatment on the sensing of a nutrition gradient. Therefore, we analyzed the effects in chemotaxis migration assay. The cells follow an FCS gradient without restriction on their path. The forward migration index (FMI) and the velocity of SKOV3 cells were not reduced by Miu pre-treatment. These data, together with the finding of unimpaired secretion, detected by HRP secretion assay, indicate no influence of treatment on the sensing of a nutrition gradient. The migration of cancer cells is dependent on transport and secretion processes from the nucleus to the plasma membrane.[65,106] As an example, integrin and growth factor receptors were transported to the migration site for sensing nutrition and stabilizing the migration process by binding to the surface.[107,108] The intact secretion after Miu treatment further affirm the intactness of actin cytoskeleton, because actin is important in vesicle transport from nucleus to cytoplasm in the secreting cell.[108,109] In summary, the migration inhibition of Miu treated cancer cells was independent of cytoplasmic actin and indicated specific inhibition of motility exclusively in three dimensional (3D) movements.

4.3.2 Miu treatment modified the nuclear stiffness of cancer cells

Modern research focuses on the physical properties of migrating, dying or differentiating cells. The stiffness of cells and isolated organelles, such as the nucleus, has been linked to basic cellular processes.[67,110] Existing studies elucidated the alteration of cellular stiffness according to the differentiation state of cells.[111] In addition, cancer cells have softer cellular structures in comparison to non-cancer cells. The migration of cancer cells in a 3D environment is dependent on the cell rigidity and extra cellular matrix mechanics.[66] Not only cellular, but also stiffness of the nucleus can be a critical determinant of the successful migration of cancer cells.[53] Our results showed increased nuclear stiffness in cancer cells upon Miu treatment.

There are several factors, which have been described to have an impact on the stiffness of nuclei. Firstly, cytoskeletal tension influences the nuclear deformation by cytoplasmic actin dynamics and actin binding proteins.[112] Secondly, lamins anchor the chromatin to the cytoplasmic actin, which is associated to the nuclear envelope, and therefore, might stabilize the rigidity of the nuclear membrane.[113] Thirdly, the DNA condensation status and chromatin structure, which is regulated by histone acetylation and deacetylation, have an impact on the nuclear stiffness. For instance, treatment with histone deacetylase (HDAC) inhibitors, such as trichostatin A, led to the decondensation of chromatin and indicated softer nuclei.[67,110] Moreover, the inhibition of cytoplasmic myosin II with blebbistatin showed to induce stiffer nuclei in cardiac myocytes.[110]

One hypothesis for the inhibition of migration by Miu low dose treatment is the reduction of nuclear deformability.[112] Therefore, the specific effect of migration inhibition in Boyden chamber assay might be dependent on nuclear stiffness. Miu treated cells showed almost normal two dimensional (2D) migration characteristic, which was measured by chemotaxis and wound healing assay, but lost the ability of 3D migration through restricted pores. To confirm this hypothesis, cell migration properties were analyzed using 3D collagen I gels. Indeed, Miu treated cancer cells showed a lower number of deformable cells, reduced mobility, and decreased the amount of cells, which successfully squeezed through restricted pores. Accordingly, a recently published study postulated the need of a contractile perinuclear actin system for sufficient migration in a confined environment. Furthermore, the perinuclear actin protects the cells during 3D migration from apoptosis, but is probably neglectable in 2D migration.[114] In conclusion, the results pointed to an effect on 3D migration accompanied by an enhanced nuclear stiffness, which might be attributed to effects of Miu on perinuclear actin.

4.3.3 Proteome indicated an alteration of transcription factor signaling

Cytoplasmic actin disruption has been postulated to have an impact on alteration of protein signaling.[20] We performed time-course proteome analysis in order to obtain insights into affected proteins in a time-dependent manner.

In accordance with the actin staining, large alterations of proteins were recorded after early time points of Miu treatment. Those effects on protein expression due to

cytoplasmic actin disruption were described before.[20] Of note, the proteome data displayed the down-regulation of a prominent protein cluster a few hours before the effect on migration was observed. This might indicate a functional correlation of migration inhibition and the alterations of protein levels.

Notably, the pathway of lowest FDR and simultaneously an enrichment factor over two was the migration-associated Wnt-signaling pathway. Transcription factors or co-factors such as NFAT5 and p300, which are linked to the Wnt-signaling pathway, were significantly down-regulated in proteome analysis. Accordingly, we could demonstrate the inhibition of nuclear translocation of Wnt-signaling transcription factors β-catenin and NFAT5. In addition, the reduction of p300 protein level could be confirmed in further experiments. Conversely, the observation of Wnt-reporter gene assay with TCF/Lef1 promoter region indicated no transcriptional alteration after Miu treatment. One explanation could be the β-catenin independent activation of TCF/Lef1 promoter, which was previously described in hematopoietic cancer cells.[72] Independent TCF/Lef1 promoter activation was postulated before in SKOV3 cells.[115] In contrast to the alteration of β-catenin and NFAT5 translocation, the localization of p300 was not influenced, but the protein level of the transcription co-activator p300 was significantly diminished.

To our knowledge, no direct connection of Wnt-signaling and induction of nuclear stiffness exists. Wnt-pathway is, however, important in epithelial mesenchymal transition (EMT). The transformation of epithelial cells to mesenchymal phenotype enables them to migrate and disseminate to distant organs. The Wnt-signaling pathway was supposed to induce EMT in tumor cells.[116] Besides the activation of Wnt-signaling, the changes of morphology characteristics are one hallmark of EMT.[117] Cancer cells, which underwent EMT, have a softer cellular structure and higher migration potential. Consequently, this indicates a lower migration potential of cancer cells with increased cellular stiffness after inhibition of EMT.[118] There is an evidence for the alteration of EMT due to Miu treatment by disrupting Wnt-signaling-associated transcription factors, followed by increased nuclear stiffness.

4.3.4 Down-regulation of p300 linked nuclear stiffness to transcriptional alteration

With reference to the promising results of p300 down-regulation in proteome analysis and Western blot, the regulation and interaction partners of p300 were examined. Together with its functionally related partner CREB binding protein (CBP), p300 possesses acetyltransferase and transcription co-activator characteristics and is assumed to have many functions in the regulation of transcription and chromatin remodeling.[74] The enhancement of histone acetylation was previously postulated to be prominent in cancer cells, which have a high transcriptional activity, accompanied by decondensation of chromatin.[119] Accordingly, the condensation and decondensation of chromatin structure have an impact on the nuclear stiffness. We demonstrated the reduction of p300 protein level after Miu treatment, which might have led to a down-regulation of acetylation of histones and therefore to the condensation of chromatin. Although, the acetylation state of Miu treated cells, have to be tested in further investigations, the functional relation of p300 and stiffness induction is probable. One possibility is that the decrease of histone acetylation might elevate the nuclear stiffness. The contrary was postulated for the inhibition of deacetylation, which reduced the nuclear stiffness.[94,95]

Besides the alteration of histone acetylation, p300 was found to interact with the transcription co-factor MRTF. Both transcriptional co-activators synergistically promoted cell migration and the transcription of migration-related genes.[70] Indeed, we could confirm this study by the investigation of MRTF-associated proteins in proteome analysis. Notably, 14 out of 18 observed MRTF-associated proteins were down-regulated after Miu treatment, indicating a strong connection of p300 to MRTF. These data could be reinforced by the achieved down-regulation of the migration-associated gene CYR61. Furthermore, CYR61 was found to be activated by mechanical stress due to MRTF/CBP in smooth muscle cells.[120] The activation of p300-MRTF-related genes might be dependent on mechanical stress during restricted 3D migration. Miu might reduce the translocation of specific transcription factors, followed by down-regulation of p300 and a fewer acetylation of histones. This may finally increase the chromatin condensation, accompanied by the enhancement of nuclear stiffness, subsequently leading to an inhibition of migration. In conclusion, we presented an impact of mechanical alteration

after Miu treatment on protein and transcriptional level. However, more examinations on the connection of p300, nuclear stiffness and transcription factor localization are needed to conclude the exact mechanism of Miu long term treatment and inhibition of 3D cell migration.

4.4 Future perspectives

The combination of ChB with DNA damaging agent Doxo represents just the beginning of promising applications of actin binding compounds in cancer therapy. It will open an attractive field of research to find appropriate combination partners for actin binding compounds. Since actin is an ubiquitously expressed protein, it interacts with a lot of cellular compartments and signaling cascades. We could show the specific inhibition of cancer cell growth by targeting counter regulatory mechanisms, but more investigations should be performed on the function of actin and its interacting proteins.

Furthermore, optimization of chemical structure of ChB, concerning chemical synthesis and specificity could be examined. Herein, we provide Miu as an alternative to the complex synthesis of ChB. Particularly, the chemical structure of Miu is more accessible to chemical synthesis and could be easily modified. Current studies concentrate on the modification of Miu to obtain derivatives, which demonstrate the functionality on cancer cells beside prominent actin disrupting effects. Moreover, this study highly supports the assumption, that myxobacterial derived compounds such as Miu, have an impact on cellular functions beside the alteration of actin dynamics in the cytoplasm. In line with these examinations, further research should observe the evidence of physical properties on transcription regulation and the nuclear actin structures altered by actin binding compounds. Therefore ChB and Miu represent tools for further investigations of actin as a potential target.

5 SUMMARY

The cytoskeleton of cancer cells has been proved to be an attractive target for tumor therapy in patients. In contrast to the inhibition of microtubule structure with chemotherapeutic drugs like paclitaxel, the actin binding compounds have not achieved the use in clinics yet. One limiting factor for the application of actin binding compounds in patients might be the expected side effects of higher treatment concentrations. Hence, the pharmacological targeting of the actin cytoskeleton in lower treatment concentrations as well as in combination with common chemotherapeutics may represent new approaches for the use of actin binding compounds in cancer therapy. Furthermore, there is an urgent need to understand the molecular mechanism of the tested compounds to design rational therapy strategies.

This study introduces the actin binding compounds chondramide and miuraenamide as tools for the inhibition of cancer cell survival and migration. Firstly, we show the high potential of actin binding compounds to inhibit the DNA damage response after combination treatment with the topoisomerase inhibitor doxorubicin. The combination treatment of chondramide and doxorubicin displays a disruption of Golgi dependent DNA damage response and indicates the increase of DNA damage and cell death in cancer cells. Furthermore, the combination treatment has negligible effects on non-cancer cells and achieves a reduction of tumor volume *in vivo*. Secondly, we demonstrate the effect of low dose miuraenamide treatment on migration of cancer cells. The cell migration in a three dimensional environment is significantly reduced after miuraenamide treatment and is elucidated to be nuclear stiffness dependent. Furthermore, the proteome analysis indicates the inhibition of migration-related signaling in cancer cells, for instance, proteins of the Wnt-signaling pathway and MRTF/SRF-associated proteins are down-regulated after miuraenamide treatment.

In summary, this work provides evidence for the implementation of actin binding compounds in cancer therapy and shows the specific effects of the compounds on two

hallmarks of cancer, beyond simple disruption of the actin cytoskeleton. This study outlines the pro-apoptotic and anti-metastatic potential of chondramide and miuraenamide in low dose treatment. In conclusion, we evaluated novel unconventional treatment approaches in cancer for the further application of actin binding compounds.

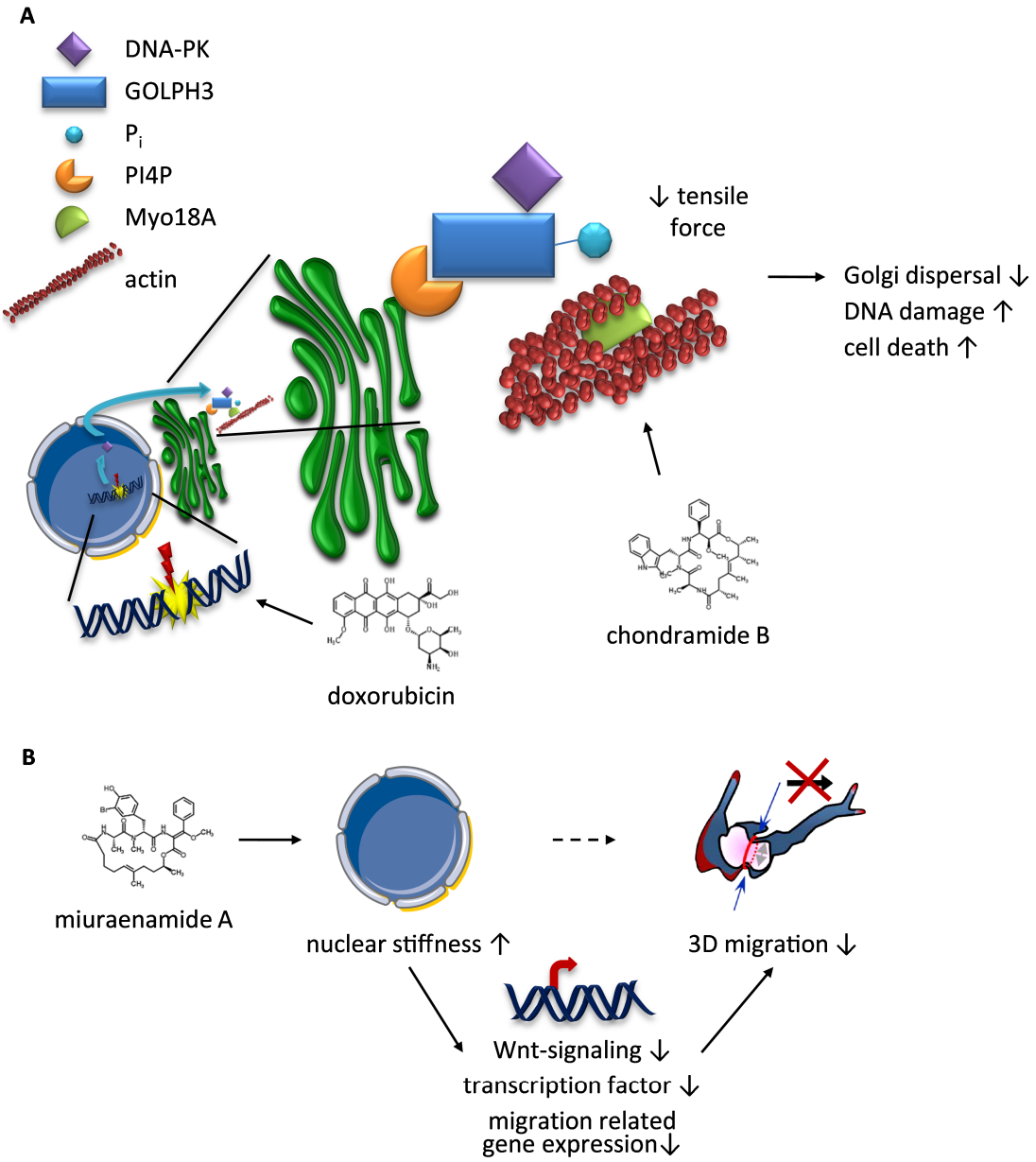

Figure 5.1: The mechanisms of chondramide B and miuraenamide A treatment. A: Inhibition mechanism of DNA damage response (DDR) by means of Golgi dispersal. Doxorubicin induces DNA double strand breaks, which further leads to the activation of Golgi dependent DDR**.** Induced Golgi dispersal is inhibited by chondramide B, causing enhanced DNA damage and cell death in cancer cells. **B:** The increased nuclear stiffness and the alteration of transcription signaling after miuraenamide A treatment leads to migration inhibition. The treatment with miuraenamide A has an impact on transcription factors in Wnt-signaling pathway, and reduces migration-related gene expression, which is followed by the reduction of three dimensional (3D) cell migration.

6 REFERENCES

1 Torre, L. A. *et al.* Global cancer statistics, 2012. *CA Cancer J Clin* **65**, 87-108 (2015).
2 Stewart, B. W. & Wild, C. P. World Cancer Report 2014. *International Agency for Research on Cancer* (2014).
3 Vorobiof, D. A. Recent advances in the medical treatment of breast cancer. *F1000Res* **5**, 2786 (2016).
4 Jackisch, C. *et al.* Evolving landscape of human epidermal growth factor receptor 2-positive breast cancer treatment and the future of biosimilars. *Breast* **32**, 199-216 (2017).
5 Tashiro, H. & Brenner, M. K. Immunotherapy against cancer-related viruses. *Cell Res* **27**, 59-73 (2017).
6 Mamounas, E. P. *et al.* Paclitaxel after doxorubicin plus cyclophosphamide as adjuvant chemotherapy for node-positive breast cancer: results from NSABP B-28. *J Clin Oncol* **23**, 3686-3696 (2005).
7 Hanahan, D. & Weinberg, R. A. The hallmarks of cancer. *Cell* **100**, 57-70 (2000).
8 Judson, I. *et al.* Doxorubicin alone versus intensified doxorubicin plus ifosfamide for first-line treatment of advanced or metastatic soft-tissue sarcoma: a randomised controlled phase 3 trial. *Lancet Oncol* **15**, 415-423 (2014).
9 McGowan, J. V. *et al.* Anthracycline Chemotherapy and Cardiotoxicity. *Cardiovasc Drugs Ther* (2017).
10 Gornstein, E. & Schwarz, T. L. The paradox of paclitaxel neurotoxicity: Mechanisms and unanswered questions. *Neuropharmacology* **76 Pt A**, 175-183 (2014).
11 Chaffer, C. L. & Weinberg, R. A. A perspective on cancer cell metastasis. *Science* **331**, 1559-1564 (2011).
12 Zhang, S. *et al.* SRC family kinases as novel therapeutic targets to treat breast cancer brain metastases. *Cancer Res* **73**, 5764-5774 (2013).
13 Stupp, R. *et al.* Cilengitide combined with standard treatment for patients with newly diagnosed glioblastoma with methylated MGMT promoter (CENTRIC EORTC 26071-22072 study): a multicentre, randomised, open-label, phase 3 trial. *Lancet Oncol* **15**, 1100-1108 (2014).
14 Steeg, P. S. Targeting metastasis. *Nat Rev Cancer* **16**, 201-218 (2016).
15 Cooper, J. A. & Schafer, D. A. Control of actin assembly and disassembly at filament ends. *Curr Opin Cell Biol* **12**, 97-103 (2000).
16 Perrin, B. J. & Ervasti, J. M. The actin gene family: function follows isoform. *Cytoskeleton (Hoboken)* **67**, 630-634 (2010).
17 Pollard, T. D. & Cooper, J. A. Actin, a central player in cell shape and movement. *Science* **326**, 1208-1212 (2009).
18 Scheer, U. *et al.* Microinjection of actin-binding proteins and actin antibodies demonstrates involvement of nuclear actin in transcription of lampbrush chromosomes. *Cell* **39**, 111-122 (1984).

19 Hofmann, W. *et al.* Cofactor requirements for nuclear export of Rev response element (RRE)- and constitutive transport element (CTE)-containing retroviral RNAs. An unexpected role for actin. *J Cell Biol* **152**, 895-910 (2001).
20 Miralles, F. *et al.* Actin dynamics control SRF activity by regulation of its coactivator MAL. *Cell* **113**, 329-342 (2003).
21 Olave, I. A. *et al.* Nuclear actin and actin-related proteins in chromatin remodeling. *Annu Rev Biochem* **71**, 755-781 (2002).
22 Cairns, B. R. *et al.* Two actin-related proteins are shared functional components of the chromatin-remodeling complexes RSC and SWI/SNF. *Mol Cell* **2**, 639-651 (1998).
23 Belin, B. J. *et al.* DNA damage induces nuclear actin filament assembly by Formin -2 and Spire-(1/2) that promotes efficient DNA repair. [corrected]. *Elife* **4**, e07735 (2015).
24 Sheterline, P. *et al.* The nature and regulation of actin filament turnover in cells. *Acta Histochem Suppl* **41**, 303-309 (1991).
25 Pollard, T. D. *et al.* Molecular mechanisms controlling actin filament dynamics in nonmuscle cells. *Annu Rev Biophys Biomol Struct* **29**, 545-576 (2000).
26 Korn, E. D. Actin polymerization and its regulation by proteins from nonmuscle cells. *Physiol Rev* **62**, 672-737 (1982).
27 Cooper, J. A. Effects of cytochalasin and phalloidin on actin. *J Cell Biol* **105**, 1473-1478 (1987).
28 Harvey, A. L. Natural products in drug discovery. *Drug Discov Today* **13**, 894-901 (2008).
29 Li, J. W. & Vederas, J. C. Drug discovery and natural products: end of an era or an endless frontier? *Science* **325**, 161-165 (2009).
30 Reichenbach, H. & Hofle, G. Biologically active secondary metabolites from myxobacteria. *Biotechnol Adv* **11**, 219-277 (1993).
31 Bollag, D. M. *et al.* Epothilones, a new class of microtubule-stabilizing agents with a taxol-like mechanism of action. *Cancer Res* **55**, 2325-2333 (1995).
32 Sasse, F. *et al.* The chondramides: cytostatic agents from myxobacteria acting on the actin cytoskeleton. *J Natl Cancer Inst* **90**, 1559-1563 (1998).
33 Foerster, F. *et al.* Targeting the actin cytoskeleton: selective antitumor action via trapping PKCvarepsilon. *Cell Death Dis* **5**, e1398 (2014).
34 Menhofer, M. H. *et al.* The actin targeting compound Chondramide inhibits breast cancer metastasis via reduction of cellular contractility. *PLoS One* **9**, e112542 (2014).
35 Iizuka, T. *et al.* Miuraenamides A and B, novel antimicrobial cyclic depsipeptides from a new slightly halophilic myxobacterium: taxonomy, production, and biological properties. *J Antibiot (Tokyo)* **59**, 385-391 (2006).
36 Sumiya, E. *et al.* Cell-morphology profiling of a natural product library identifies bisebromoamide and miuraenamide A as actin filament stabilizers. *ACS Chem Biol* **6**, 425-431 (2011).
37 Karmann, L. *et al.* Totalsynthese und biologische Evaluierung von Miuraenamiden. *Angewandte Chemie* **127**, 4585-4590 (2015).
38 Weissman, K. J. & Muller, R. Myxobacterial secondary metabolites: bioactivities and modes-of-action. *Nat Prod Rep* **27**, 1276-1295 (2010).
39 Liu, L. F. *et al.* Type II DNA topoisomerases: enzymes that can unknot a topologically knotted DNA molecule via a reversible double-strand break. *Cell* **19**, 697-707 (1980).

40 Tewey, K. M. *et al.* Intercalative antitumor drugs interfere with the breakage-reunion reaction of mammalian DNA topoisomerase II. *J Biol Chem* **259**, 9182-9187 (1984).
41 Khanna, K. K. & Jackson, S. P. DNA double-strand breaks: signaling, repair and the cancer connection. *Nat Genet* **27**, 247-254 (2001).
42 d'Adda di Fagagna, F. *et al.* Effects of DNA nonhomologous end-joining factors on telomere length and chromosomal stability in mammalian cells. *Curr Biol* **11**, 1192-1196 (2001).
43 Farber-Katz, S. E. *et al.* DNA damage triggers Golgi dispersal via DNA-PK and GOLPH3. *Cell* **156**, 413-427 (2014).
44 Pouliliou, S. & Koukourakis, M. I. Gamma histone 2AX (gamma-H2AX)as a predictive tool in radiation oncology. *Biomarkers* **19**, 167-180 (2014).
45 Dippold, H. C. *et al.* GOLPH3 bridges phosphatidylinositol-4- phosphate and actomyosin to stretch and shape the Golgi to promote budding. *Cell* **139**, 337-351 (2009).
46 Sechi, S. *et al.* The multiple cellular functions of the oncoprotein Golgi phosphoprotein 3. *Oncotarget* **6**, 3493-3506 (2015).
47 Arcamone, F. *et al.* Adriamycin, 14-hydroxydaunomycin, a new antitumor antibiotic from S. peucetius var. caesius. *Biotechnol Bioeng* **11**, 1101-1110 (1969).
48 Turley, H. *et al.* The distribution and expression of the two isoforms of DNA topoisomerase II in normal and neoplastic human tissues. *Br J Cancer* **75**, 1340-1346 (1997).
49 Berthiaume, J. M. & Wallace, K. B. Adriamycin-induced oxidative mitochondrial cardiotoxicity. *Cell Biol Toxicol* **23**, 15-25 (2007).
50 Lauffenburger, D. A. & Horwitz, A. F. Cell migration: a physically integrated molecular process. *Cell* **84**, 359-369 (1996).
51 Wolf, K. *et al.* Compensation mechanism in tumor cell migration: mesenchymal-amoeboid transition after blocking of pericellular proteolysis. *J Cell Biol* **160**, 267-277 (2003).
52 Mitchison, T. J. & Cramer, L. P. Actin-based cell motility and cell locomotion. *Cell* **84**, 371-379 (1996).
53 Krause, M. & Wolf, K. Cancer cell migration in 3D tissue: negotiating space by proteolysis and nuclear deformability. *Cell Adh Migr* **9**, 357-366 (2015).
54 Nicoletti, I. *et al.* A rapid and simple method for measuring thymocyte apoptosis by propidium iodide staining and flow cytometry. *J Immunol Methods* **139**, 271-279 (1991).
55 Bradford, M. M. A rapid and sensitive method for the quantitation of microgram quantities of protein utilizing the principle of protein-dye binding. *Anal Biochem* **72**, 248-254 (1976).
56 Ladner, C. L. *et al.* Visible fluorescent detection of proteins in polyacrylamide gels without staining. *Anal Biochem* **326**, 13-20 (2004).
57 Zeidman, R. *et al.* Protein kinase Cepsilon actin-binding site is important for neurite outgrowth during neuronal differentiation. *Mol Biol Cell* **13**, 12-24 (2002).
58 Brady, H. J. M. *Apoptosis methods and protocols*. (Humana Press, 2004).
59 Webb, J. L. Effect of more than one inhibitor, antagonism, summation, and synergism. *Enzyme and Metabolic Inhibitors. New York: Academic Press*, 488-512 (1963).

60 Benjamini, Y. & Hochberg, Y. Controlling the False Discovery Rate: A Practical and Powerful Approach to Multiple Testing. *Journal of the Royal Statistical Society. Series B (Methodological)* **57**, 289-300 (1995).

61 Rupes, I. *et al.* G2/M arrest caused by actin disruption is a manifestation of the cell size checkpoint in fission yeast. *Mol Biol Cell* **12**, 3892-3903 (2001).

62 Green, R. A. *et al.* Cytokinesis in animal cells. *Annu Rev Cell Dev Biol* **28**, 29-58 (2012).

63 Parsons, J. T. *et al.* Cell adhesion: integrating cytoskeletal dynamics and cellular tension. *Nat Rev Mol Cell Biol* **11**, 633-643 (2010).

64 von Blume, J. *et al.* Actin remodeling by ADF/cofilin is required for cargo sorting at the trans-Golgi network. *J Cell Biol* **187**, 1055-1069 (2009).

65 Park, S. J. *et al.* Estradiol, TGF-beta1 and hypoxia promote breast cancer stemness and EMT-mediated breast cancer migration. *Oncol Lett* **11**, 1895-1902 (2016).

66 Paszek, M. J. *et al.* Tensional homeostasis and the malignant phenotype. *Cancer Cell* **8**, 241-254 (2005).

67 Krause, M. *et al.* Probing the compressibility of tumor cell nuclei by combined atomic force-confocal microscopy. *Phys Biol* **10**, 065002 (2013).

68 Vigorito, E. *et al.* RhoG regulates gene expression and the actin cytoskeleton in lymphocytes. *Oncogene* **22**, 330-342 (2003).

69 Rivas, F. V. *et al.* Actin cytoskeleton regulates calcium dynamics and NFAT nuclear duration. *Mol Cell Biol* **24**, 1628-1639 (2004).

70 He, H. *et al.* Transcriptional factors p300 and MRTF-A synergistically enhance the expression of migration-related genes in MCF-7 breast cancer cells. *Biochem Biophys Res Commun* **467**, 813-820 (2015).

71 MacDonald, B. T. *et al.* Wnt/beta-catenin signaling: components, mechanisms, and diseases. *Dev Cell* **17**, 9-26 (2009).

72 Grumolato, L. *et al.* beta-Catenin-independent activation of TCF1/LEF1 in human hematopoietic tumor cells through interaction with ATF2 transcription factors. *PLoS Genet* **9**, e1003603 (2013).

73 Saneyoshi, T. *et al.* The Wnt/calcium pathway activates NF-AT and promotes ventral cell fate in Xenopus embryos. *Nature* **417**, 295-299 (2002).

74 Ogryzko, V. V. *et al.* The transcriptional coactivators p300 and CBP are histone acetyltransferases. *Cell* **87**, 953-959 (1996).

75 Hecht, A. *et al.* The p300/CBP acetyltransferases function as transcriptional coactivators of beta-catenin in vertebrates. *EMBO J* **19**, 1839-1850 (2000).

76 Rebhan, M. *et al. GeneCards: integrating information about genes, proteins and diseases*, <http://www.genecards.org/Search/Keyword?queryString=Mrtf> (1997).

77 Leitner, L. *et al.* Epithelial Protein Lost in Neoplasm alpha (Eplin-alpha) is transcriptionally regulated by G-actin and MAL/MRTF coactivators. *Mol Cancer* **9**, 60 (2010).

78 Luo, X. G. *et al.* Histone methyltransferase SMYD3 promotes MRTF-A-mediated transactivation of MYL9 and migration of MCF-7 breast cancer cells. *Cancer Lett* **344**, 129-137 (2014).

79 Zhu, L. Y. *et al.* Silencing of MICAL-L2 suppresses malignancy of ovarian cancer by inducing mesenchymal-epithelial transition. *Cancer Lett* **363**, 71-82 (2015).

80 Pawlowski, R. *et al.* An actin-regulated importin alpha/beta-dependent extended bipartite NLS directs nuclear import of MRTF-A. *EMBO J* **29**, 3448-3458 (2010).

81 Cocco, G. *et al.* Colchicine in clinical medicine. A guide for internists. *Eur J Intern Med* **21**, 503-508 (2010).
82 Zahreddine, H. & Borden, K. L. Mechanisms and insights into drug resistance in cancer. *Front Pharmacol* **4**, 28 (2013).
83 Peters, G. J. *et al.* Basis for effective combination cancer chemotherapy with antimetabolites. *Pharmacol Ther* **87**, 227-253 (2000).
84 Prokhorova, E. A. *et al.* Role of the nucleus in apoptosis: signaling and execution. *Cell Mol Life Sci* **72**, 4593-4612 (2015).
85 Zhu, K. *et al.* GOLPH3 overexpression correlates with poor response to neoadjuvant therapy and prognosis in locally advanced rectal cancer. *Oncotarget* **7**, 68328-68338 (2016).
86 Tang, W. *et al.* Overexpression of GOLPH3 is associated with poor survival in Non-small-cell lung cancer. *Am J Transl Res* **8**, 1756-1762 (2016).
87 Abd El-Maqsoud, N. M. *et al.* Golgi Phosphoprotein-3 and Y-Box-Binding Protein-1 Are Novel Markers Correlating With Poor Prognosis in Prostate Cancer. *Clin Genitourin Cancer* **14**, e143-152 (2016).
88 Scott, K. L. & Chin, L. Signaling from the Golgi: mechanisms and models for Golgi phosphoprotein 3-mediated oncogenesis. *Clin Cancer Res* **16**, 2229-2234 (2010).
89 Bishe, B. *et al.* Role of phosphatidylinositol 4-phosphate (PI4P) and its binding protein GOLPH3 in hepatitis C virus secretion. *J Biol Chem* **287**, 27637-27647 (2012).
90 Tu, L. *et al.* Signal-mediated dynamic retention of glycosyltransferases in the Golgi. *Science* **321**, 404-407 (2008).
91 Takahashi, M. *et al.* Role of N-glycans in growth factor signaling. *Glycoconj J* **20**, 207-212 (2004).
92 Weber, A. N. *et al.* Four N-linked glycosylation sites in human toll-like receptor 2 cooperate to direct efficient biosynthesis and secretion. *J Biol Chem* **279**, 34589-34594 (2004).
93 Harberts, E. & Gaspari, A. A. TLR signaling and DNA repair: are they associated? *J Invest Dermatol* **133**, 296-302 (2013).
94 Miura, Y. *et al.* O-GlcNAc modification affects the ATM-mediated DNA damage response. *Biochim Biophys Acta* **1820**, 1678-1685, doi:10.1016/j.bbagen.2012.06.013 (2012).
95 Zachara, N. E. *et al.* The dynamic stress-induced "O-GlcNAc-ome" highlights functions for O-GlcNAc in regulating DNA damage/repair and other cellular pathways. *Amino Acids* **40**, 793-808, doi:10.1007/s00726-010-0695-z (2011).
96 Wahba, A. *et al.* Polysome Profiling Links Translational Control to the Radioresponse of Glioblastoma Stem-like Cells. *Cancer Res* **76**, 3078-3087 (2016).
97 Fisher, B. *et al.* Tamoxifen and chemotherapy for lymph node-negative, estrogen receptor-positive breast cancer. *J Natl Cancer Inst* **89**, 1673-1682 (1997).
98 Osborne, C. K. Steroid hormone receptors in breast cancer management. *Breast Cancer Res Treat* **51**, 227-238 (1998).
99 Schweikart, K. *et al.* The effects of jaspamide on human cardiomyocyte function and cardiac ion channel activity. *Toxicol In Vitro* **27**, 745-751 (2013).
100 Calloe, K. *et al.* KCNQ channels are involved in the regulatory volume decrease response in primary neonatal rat cardiomyocytes. *Biochim Biophys Acta* **1773**, 764-773 (2007).

101 Wang, Y. *et al.* Over-expression of calpastatin aggravates cardiotoxicity induced by doxorubicin. *Cardiovasc Res* **98**, 381-390 (2013).
102 Yamada, T. *et al.* Induction of fatty streak-like lesions in vitro using a culture model system simulating arterial intima. *Am J Pathol* **141**, 1435-1444 (1992).
103 Damrot, J. *et al.* Lovastatin protects human endothelial cells from the genotoxic and cytotoxic effects of the anticancer drugs doxorubicin and etoposide. *Br J Pharmacol* **149**, 988-997 (2006).
104 Hayot, C. *et al.* Characterization of the activities of actin-affecting drugs on tumor cell migration. *Toxicol Appl Pharmacol* **211**, 30-40 (2006).
105 Lazaro-Dieguez, F. *et al.* Dynamics of an F-actin aggresome generated by the actin-stabilizing toxin jasplakinolide. *J Cell Sci* **121**, 1415-1425 (2008).
106 Dumitriu, I. E. *et al.* The secretion of HMGB1 is required for the migration of maturing dendritic cells. *J Leukoc Biol* **81**, 84-91 (2007).
107 Tamatani, T. *et al.* Hepatocyte growth factor is an invasion/migration factor of rat urothelial carcinoma cells in vitro. *Carcinogenesis* **20**, 957-962 (1999).
108 Shen, X. *et al.* Brefeldin A-inhibited ADP-ribosylation factor activator BIG2 regulates cell migration via integrin beta1 cycling and actin remodeling. *Proc Natl Acad Sci U S A* **109**, 14464-14469 (2012).
109 Trifaro, J. M. *et al.* Cytoskeleton and molecular mechanisms in neurotransmitter release by neurosecretory cells. *Eur J Pharmacol* **225**, 83-104 (1992).
110 Lee, H. *et al.* Cytoskeletal prestress regulates nuclear shape and stiffness in cardiac myocytes. *Exp Biol Med (Maywood)* **240**, 1543-1554 (2015).
111 Heo, S. J. *et al.* Differentiation alters stem cell nuclear architecture, mechanics, and mechano-sensitivity. *Elife* **5** (2016).
112 Thiam, H. R. *et al.* Perinuclear Arp2/3-driven actin polymerization enables nuclear deformation to facilitate cell migration through complex environments. *Nat Commun* **7**, 10997 (2016).
113 Lammerding, J. *et al.* Lamins A and C but not lamin B1 regulate nuclear mechanics. *J Biol Chem* **281**, 25768-25780 (2006).
114 Skau, C. T. *et al.* FMN2 Makes Perinuclear Actin to Protect Nuclei during Confined Migration and Promote Metastasis. *Cell* **167**, 1571-1585 e1518 (2016).
115 Usongo, M. *et al.* Activation of the canonical WNT signaling pathway promotes ovarian surface epithelial proliferation without inducing beta-catenin/Tcf-mediated reporter expression. *Dev Dyn* **242**, 291-300 (2013).
116 Kalluri, R. & Weinberg, R. A. The basics of epithelial-mesenchymal transition. *J Clin Invest* **119**, 1420-1428 (2009).
117 Yang, J. *et al.* Twist, a master regulator of morphogenesis, plays an essential role in tumor metastasis. *Cell* **117**, 927-939 (2004).
118 Osborne, L. D. *et al.* TGF-beta regulates LARG and GEF-H1 during EMT to affect stiffening response to force and cell invasion. *Mol Biol Cell* **25**, 3528-3540 (2014).
119 Janmey, P. A. *et al.* From tissue mechanics to transcription factors. *Differentiation* **86**, 112-120 (2013).
120 Hanna, M. *et al.* Mechanical regulation of the proangiogenic factor CCN1/CYR61 gene requires the combined activities of MRTF-A and CREB-binding protein histone acetyltransferase. *J Biol Chem* **284**, 23125-23136 (2009).

7 APPENDIX

7.1 Abbreviations

2D	Two dimensional
3D	Three dimensional
AFM	Atomic force microscope
ANOVA	Analysis of variance between groups
ATM	Ataxia-telangiectasia mutated
ATP/ADP	Adenosine triphosphate/diphosphate
ATR	ATM- and RAD3-related
BSA	Bovine serum albumin
cDNA	Complementary DNA
ChB	Chondramide B
DDR	DNA damage response
DDS	DNA double strand
DMEM	Dulbecco‘s Modified Eagle Medium
DMSO	Dimethylsulfoxide
DNA	Desoxyribunucleic acid
DNA-PK	DNA-dependent protein kinase
Doxo	Doxorubicin
DSB	DNA double strand breaks
e. g.	For example
ECGM	endothelial cell growth medium
ECL	Enhanced chemiluminescence
ECM	Extracellular matrix
EDTA	Ethylenediaminetetraacetic acid
FACS	Fluorescence-activated cell sorting
F-actin	Filamentous actin
FCS	Fetal calf serum
FDR	False discovery rate
G-actin	Globular actin
GAPDH	Glyceraldehyde 3-phosphate dehydrogenase
GM130	Golgi matrix protein 130 kDa
GOLPH3	Golgi phosphoprotein 3
HFS	Hypotonic fluorochrome solution

HRP	Horseradish peroxidase
HUVEC	Human umbilical vein endothelial cell
IgG	Immunoglobulin G
mRNA	Messenger ribonucleic acid
MRTF-A	Myocardin-related transcription factor-A
Myo18A	Myosin 18A
NADH	Nicotinamide adenine dinucleotide H
NFAT	Nuclear factor of activated T-cells
no.	Number
o/n	Overnight
PARP	Poly (ADP-ribose) polymerase
PBS	Phosphate buffered saline
PI	Propidium iodide
PI4P	Phosphatidylinositol-4-phosphate
PKCε	Protein kinase C ε
PMSF	Phenylmethanesulfonylfluoride
PVDF	Polyvinylidene difluoride
ROS	Reactive oxygen species
rpm	Revolutions per minute
RPMI	Roswell Park Memorial Institute
RT	Room temperature
SDS	Sodium dodecyl sulfate
SEM	Standard error of the mean
Src	Sarcoma
SRF	Serum response factor
T/E	Trypsin/EDTA
TBS-T	Tris-buffered saline and Tween 20
Thr	Threonine
YP	Yo-Pro-1
γH2A.x	Phospho-histone 2A.x

7.2 Units

°C	Celsius degree
A	Ampere
Da	Dalton
g	Gram
H	Hour
Hz	Hertz
l	Liter
m	Meter
M	Molar (mol/l)
min	Minute
N	Newton
Pa	Pascal
V	Volt
W	Watt

7.3 Publications

7.3.1 Original publications

Targeting the Actin Cytoskeleton: Selective Anti-Tumor Action via Trapping PKCε
Foerster F., Braig S., Moser C., Kubisch R., Busse J., Wagner E., Schmoeckel E., Mayr D., Schmitt S., Huettel S., Mueller R. and Vollmar A.M.
Cell Death & Disease. 2014, August 28.

Therapeutic Application of Actin binding Chondramide and the Established Chemotherapeutic Doxorubicin
Moser C.*, Foerster F.*, Ramanujam D., Krieg A., Kubisch-Dohmen R., BusseJ, Wagner E, Engelhardt S., Mueller R. and Vollmar A.M.
In preparation

Migration Inhibition by Actin Binding Compounds – Targeting Deformation Ability of Cancer Cells
Moser C., Ruediger D., Yu P., Kuester B., Kazmaier U., Vollmar A.M. and Zahler S.
In preparation

7.3.2 Poster presentations

Migration Inhibition by Actin Binding Compounds - Beyond Simple Actin Polymerization
Moser C., Kazmaier U., Vollmar A.M., Zahler S.
Deutsche Pharmazeutische Gesellschaft (DPhG) Annual Meeting 2016, October 4-7, 2016, Munich, Germany

Tumor Sensitization to the DNA Damaging Agent Doxorubicin by the Actin Nucleator Chondramide
Moser C., Foerster F., Wagner E., Mueller R., Vollmar A.M.
Actin in Action: From Molecules to Cellular Functions, September 7-10, 2016, Heidelberg, Germany

Myxobacterial Compound Chondramide in a Therapeutic Approach Towards Novel Combination Treatment of Actin Binding Agents and Doxorubicin in Cancer Therapy
Moser C., Foerster F., Wagner E., Mueller R., Vollmar A.M.
2nd European Conference on Natural Products, September 6-9, 2015, Frankfurt a. M., Germany

Targeting the DNA Damage Repair in Cancer via the Actin Cytoskeleton. Synergistic Effects of Chemotherapeutic Combination of Myxobacterial Chondramide and Doxorubicin
Moser C., Foerster F., Wagner E., Mueller R., Vollmar A.M.
5th HIPS Symposium, July 2, 2015, Saarbruecken, Germany

7.3.3 Oral presentations

Additional Effects of Miuraenamide Besides the Actin Hyperpolymerization
Moser C., Vollmar A.M., Zahler S.
FOR 1406 Meeting, July 5, 2016, Munich, Germany

Synergistic Effects of Chemotherapeutic Combination of Chondramide and Doxorubicin
Moser C., Foerster F., Wagner E., Mueller R., Vollmar A.M.
FOR 1406 Meeting, June 30-July 1, 2015, Saarbruecken, Germany

Chondramide Combination Treatment in Cancer Cells
Moser C., Foerster F., Wagner E., Mueller R., Vollmar A.M.
FOR 1406 Meeting, January 8, 2015, Munich, Germany

7.4 Acknowledgement

Mein allergrößter Dank geht an Frau Prof. Dr. Vollmar für die Möglichkeit am Lehrstuhl für Pharmazeutische Biologie meine Dissertation anfertigen zu können. Ich möchte mich ebenso dafür bedanken, dass ich Konferenzen besuchen durfte und dafür, ein Teil der FOR 1406 gewesen zu sein. Vielen Dank für die umfassende Betreuung, die wertvollen Diskussionen und Ihre herzliche Art.

Des Weiteren möchte ich Ihnen, Herrn Prof. Dr. Zahler danken, dass Sie mich im letzten Abschnitt meiner Doktorarbeit betreut haben, Sie sich bereit erklärt haben als Zweitgutachter für meine Dissertation zur Verfügung zu stehen und dafür, dass Ihre Tür für Fragen und Anregungen immer offen stand. Ebenso danke ich Ihnen für die konstruktiven Gespräche, die technischen Einweisungen, sowie für die zielführenden Ideen.

Ebenfalls einen herzlichen Dank an die restliche Prüfungskommission, namentlich Herrn Prof. Dr. Wahl-Schott, Herrn PD. Dr. Michalakis, Herrn PD. Dr. Dr. Grimm und Herrn Prof. Dr. Wagner, für das Interesse an meiner Arbeit und den zusätzlichen Zeitaufwand.

Mitunter das größte Dankeschön geht an meinen wissenschaftlichen Mentor Herr Dr. Florian Förster. Du hattest immer ein offenes Ohr, eine neue Eingebung bei vermeintlich unlösbaren Problemen und sowohl fachlich als auch zwischenmenschlich einen Ratschlag für mich. Deine motivierende Art hat mich immer wieder positiv gestimmt und über die Jahre meiner Doktorarbeit begleitet.

Vielen Dank auch an unsere Kooperationspartner: Prof. Dr. Müller und Prof. Dr. Kazmaier vom Helmholz-Institut für Pharmazeutische Forschung, sowie dem Institut für Organische Chemie an der Saarland Universität, für die Bereitstellung meiner Forschungssubstanzen und die Einführung in die Kultur des Saarlandes. Prof. Dr. Fürst und Dr. Iris Bischoff für die Möglichkeit eine neue Technik in Ihrem Labor zu erlernen. Prof. Dr. Dr. Engelhardt und Dr. Ramanujam vom Institut für Pharmakologie und Toxikologie, sowie Prof. Dr. Küster und Dr. Yu vom Lehrstuhl für Proteomik und Bioanalytik an der TU München für die Durchführung und Auswertung wichtiger Experimente. Dr. von Blume und Mehrshad Pakdel vom Max-Planck-Institut für Biochemie in Martinsried, für die ausführliche Einweisung und die Bereitstellung von Zellen. Vielen Dank auch an Daniel Rüdiger, für die Zellmessungen am AFM.

Ein weiteres Dankeschön möchte ich an Dr. Simone Braig richten, die mir zu Beginn meiner Promotion mit Rat und Tat zur Seite stand.

Ein herzlicher Dank gilt auch Alisa Krieg und Hilary Ganz, die im Rahmen dieser Arbeit ihre Masterarbeit angefertigt haben, und sehr zum Erfolg dieses Projekts beitragen konnten. Danke Euch für die locke(re)n Gespräche und sich daraus entwickelten Freundschaften.

Liebe Karin, lieber Fabi, vielen Dank für die tolle Atmosphäre in unserem Labor. Fabi, dir möchte ich für die ruhigen Stunden am Morgen und die vertrauten Gespräche am Abend danken. Karin, vielen Dank für den Austausch unterhaltsamer Laborgeschehnisse und deine direkte und ehrliche Art.

Auch dir Meli möchte ich herzlichst Danke sagen. Du warst während den drei gemeinsamen Jahren meine persönliche Stütze im Labor, hast mich immer auch ohne viele Worte verstanden und hattest bei größeren und kleineren Problemen immer einen ehrlichen Rat für mich, auch außerhalb vom Labor.

Liebe/r Fabi, Karin, Katja und Meli, vielen Dank für die zahlreichen gemeinsamen Stunden im PB III Praktikum und die angenehme Atmosphäre während der Betreuung.

Vielen Dank auch an alle, mit denen ich Konferenzen besuchen durfte und darüber hinaus viel Spaß hatte. Außerdem danke ich dem gesamten AK Vollmar für die herzliche Art, sowie Gemeinschaftlichkeit und dafür, dass ich wegen Euch jeden Tag gerne ins Labor gekommen bin und mich immer an diese Zeit erinnern werde.

Mein herzlichster Dank, gilt auch meiner Familie und Freunden für die große Unterstützung und das immerwährende Vertrauen in mich.

„MAN MUSS DAS UNMÖGLICHE VERSUCHEN, UM DAS MÖGLICHE ZU ERREICHEN.“
Hermann Hesse, (Deutscher Schriftsteller & Nobelpreisträger)

Lieber Christian, zu guter Letzt möchte ich dir von ganzem Herzen Danke sagen. Danke dafür, dass ich mit deiner Hilfe das Unmögliche möglich machen konnte und dafür, dass du immer für mich da bist.